Biomass burning at Cape Grim: exploring photochemistry using multi-scale modelling

Sarah J. Lawson[1], Martin Cope[1], Sunhee Lee[†], Ian E. Galbally[1], Zoran Ristovski[2] and Melita D. Keywood[1]

[1] Commonwealth Scientific and Industrial Research Organisation, Climate Science Centre, Aspendale, Australia

[2] International Laboratory for Air Quality & Health, Queensland University of Technology, Brisbane, Australia

[†]decreased

Correspondence to: S. J. Lawson (sarah.lawson@csiro.au)

Abstract

We have tested the ability of a high resolution chemical transport model (CTM) to reproduce biomass burning (BB) plume strikes and ozone (O_3) enhancements observed at Cape Grim in Tasmania Australia from the Robbins Island fire. The CTM has also been used to explore the contribution of near-field BB emissions and background sources to O_3 observations under conditions of complex meteorology. Using atmospheric observations, we have tested model sensitivity to meteorology, BB emission factors (EF) corresponding to low, medium and high modified combustion efficiency (MCE) and spatial variability. The use of two different meteorological models (TAPM-CTM and CCAM-CTM) varied the first (BB1) plume strike time by up to 15 hours, and duration of impact between 12 and 36 hours, and varied the second (BB2) plume duration between 50 and 57 hours. Meteorology also had a large impact on simulated O_3, with one model (TAPM-CTM) simulating 4 periods of O_3 enhancement, while the other model (CCAM) simulating only one period. Varying the BB EFs, which in turn varied the non–methane organic compound (NMOC) / oxides of nitrogen (NO_x) ratio, had a strongly non-linear impact on simulated O_3 concentration, with either destruction or production of O_3 predicted in different simulations. As shown in previous work (Lawson et al., 2015), minor rainfall events have the potential to significantly alter EF due to changes in combustion processes. Models which assume fixed EF for O_3 precursor species in an environment with

temporally or spatially variable EF may be unable to simulate the behaviour of important species such as O_3.

TAPM-CTM is used to further explore the contribution of the Robbins Island fire to the observed O_3 enhancements during BB1 and BB2. Overall, TAPM-CTM suggests the dominant source of O_3 observed at Cape Grim was aged urban air (age = 2 days), with a contribution of O_3 formed from local BB emissions.

This work shows the importance of assessing model sensitivity to meteorology and EF, and the large impact these variables can have in particular on simulated destruction or production of O_3 in regional atmospheric chemistry simulations. This work also shows the importance of using models to elucidate the contribution from different sources to atmospheric composition, where this is difficult using observations alone.

1 Introduction

Biomass burning (BB) makes a major global contribution to atmospheric trace gases and particles with ramifications for human health, air quality and climate. Directly emitted species include carbon monoxide (CO), carbon dioxide (CO_2), oxides of nitrogen (NO_x), primary organic aerosol (POA), non-methane organic compounds (NMOC) and black carbon (BC), while chemical transformations occurring in the plume over time lead to formation of secondary species such as O_3, oxygenated NMOC and secondary aerosol. Depending on a number of factors, including magnitude and duration of fire, plume rise and meteorology, the impact of BB plumes on human health, air quality and climate may be local, regional or global.

BB plumes from wildfires, prescribed burning, agricultural and trash burning can have a major impact on air quality in both urban and rural centres (Keywood et al., 2015; Luhar et al., 2008; Reisen et al., 2011; Emmons et al., 2010; Yokelson et al., 2011) and regional scale climate impacts (Andreae et al., 2002; Keywood et al., 2011b; Artaxo et al., 2013; Anderson et al., 2016). In Australia, BB from wild and prescibed fires impacts air quality in both rural and urban areas (Keywood et al., 2015; Reisen et al., 2011; Luhar et al., 2008; Keywood et al., 2011a) as well as indoor air quality (Reisen et al., 2011). More generally, as human population density increases, and as wildfires become more frequent (Flannigan et al., 2009; Keywood et al., 2011b), assessing the impact of BB on air quality and human health becomes more urgent

(Keywood et al., 2011b; Reisen et al., 2015). In particular, particles emitted from BB frequently lead to exceedances of air quality standards, and exposure to BB particles has been linked to poor health outcomes including respiratory effects, cardiovascular disease and mortality (Reisen et al., 2015; Reid et al., 2016; Dennekamp et al., 2015). There is also increasing evidence that mixing of BB emissions with urban emissions results in enhanced photochemistry and production of secondary pollutants such as secondary aerosol and O_3 (Jaffe and Wigder, 2012; Akagi et al., 2013; Hecobian et al., 2012), which may result in more significant health impacts than exposure to unmixed BB or urban emissions.

To be able to accurately predict and assess the impact of BB on human health, air quality and climate, models must be able to realistically simulate the chemical and microphysical processes that occur in a plume as well as plume transport and dispersion. In the case of BB plumes close to an urban centre or other sensitive receptor, models can be used to mitigate risks on community by forecasting where and when a BB plume will impact, the concentrations of toxic trace gases and particles in the plume, and potential impact of the BB plume mixing with other sources. Models also allow investigation of the contributions from BB and other sources on observed air quality when multiple sources are contributing. Understanding the relative importance of different sources is required when formulating policy decisions to improve air quality.

Lagrangian parcel models are often used to investigate photochemical transformations in BB plumes as they are transported and diluted downwind (Jost et al., 2003; Trentmann et al., 2005; Mason et al., 2006; Alvarado and Prinn, 2009; Alvarado et al., 2015) while three-dimensional (3D) Eulerian grid models have been used to investigate transport and dispersion of plumes, plume age, as well as contributions from different sources. 3D Eulerian grid models vary from fine spatial resolution on order of a few kilometers (Luhar et al., 2008; Keywood et al., 2015; Alvarado et al., 2009; Lei et al., 2013) to a resolution of up to hundreds of kilometers in global models (Arnold et al., 2015; Parrington et al., 2012).

Sensitivity studies have allowed the influence of different model components (emissions, plume rise, transport, chemistry) on model output to be investigated. Such studies are particularly important in formation of secondary species such as O_3 which have a non-linear relationship with emissions. Studies have found that modelled O_3 concentration from BB emissions is highly dependant on a range of factors including a) meteorology (plume transport and dispersion) in global (Arnold et al., 2015) and high resolution (Lei et al., 2013) Eulerian grid models, b) absolute emissions/biomass burned (Pacifico et al., 2015; Parrington et al.,

2012), c) model grid size resulting in different degrees of plume dilution (Alvarado et al., 2009), and oxidative photochemical reaction mechanisms in Lagrangian parcel models (Mason et al., 2006).

Broadly speaking, models used for simulating BB plumes comprise a) description of the emissions source b) a determination of plume rise c) treatment of the vertical transport and dispersion and d) a mechanism for simulating chemical transformations in the plume (Goodrick et al., 2013). There are challenges associated with accurately representing each of these components in BB modelling. The description of emissions source includes a spatial and temporal description of the area burnt, the fuel load, combustion completeness, and trace gas and aerosol emission factors (mass of species emitted per mass of fuel burned). The area burned is often determined by a combination of hotspot and fire scar data, determined from retrievals from satellite (Kaiser et al., 2012; Reid et al., 2009; (Giglio et al., 2013)). Cloud cover may lead to difficulties in obtaining area burnt data, while scars from small fires may be difficult to discern against complex terrain, and low intensity fires may not correspond with a detectable hotspot (Meyer et al., 2008). Emission factors are determined experimentally either by field or laboratory measurements, and are typically grouped by biome type. In some regions, such as SE Australia, biomes have been sparsely characterised (Lawson et al., 2015). Furthermore, models use biome–averaged EF which do not account for complex intra-biome variation in EF as a result of temporal and spatial differences in environmental variables. This includes factors such as impact of vegetation structure, monthly average rainfall (van Leeuwen and van der Werf, 2011) and the influence of short term rainfall events (Lawson et al., 2015). For example, EFs have been shown to vary significantly with fuel moisture which can vary seasonally (Korontzi et al., 2003;Urbanski, 2013). There may be significant spatial variability in emission factors within a biome (Castellanos et al., 2014); taken along with temporal variability, this has been shown to have a large impact on simulated concentrations of BB species in global-scale modelling (van Leeuwen et al., 2013).

Finally, the very complex mixture of trace gases and aerosols in BB plumes creates analytical challenges in quantifying EF, especially for semi and low volatility organics which are challenging to measure and identify but contribute significantly to secondary aerosol formation and photochemistry within the plume (Alvarado and Prinn, 2009; Alvarado et al., 2015; Ortega et al., 2013).

Plume rise is a description of how high the buoyant smoke plume rises above the fire, and consequently the initial vertical distribution of trace gases and aerosols in the plume (Freitas

et al., 2007). This is still a large area of uncertainty in BB models, with a generalised plume rise approach typically used which may include either homogenous mixing, prescribed fractions of emissions distributed according to mixing height, use of parametisations, and finally plume rise calculated according to atmospheric dynamics. A key driver of this uncertainty is the complexity of fire behaviour resulting in high spatial and temporal variability of pollutant and heat release, which drives variability in plume rise behaviour, such as multiple updraft cores (Goodrick et al., 2013).

Transport and dilution in models is driven by meteorology, particularly wind speed and direction, wind shear and atmospheric stability. Meteorology has a large impact on the ability of models to simulate the timing and magnitude and even composition of BB plume impacts in both local and regional scale models (Lei et al., 2013; Luhar et al., 2008; Arnold et al., 2015). For example, too-high wind speeds can lead to modelled pollutant levels which are lower than observed (e.g. Lei et al., 2013) while small deviations in wind direction lead to large concentration differences between modelled and observed, particularly when modelling emissions of multiple spatially diverse fires (Luhar et al., 2008). Dilution of BB emissions in large grid boxes in global models may also lead to discrepancies between modelled and observed NO_x, O_3 and aerosols (Alvarado et al., 2009).

Finally, models use a variety of gas-phase and aerosol-phase physical and chemical schemes, which vary in their ability to accurately represent chemical transformations, including formation of O_3 and organic aerosol (Alvarado and Prinn, 2009; Alvarado et al., 2015). Validating and constraining chemical transformations in models requires high quality, high time resolution BB observations of a wide range of trace gas and aerosol species, including important but infrequently measured species such as OH and semi volatile and low volatility NMOC. Field observations, whilst often temporally and spatially scarce, are particularly valuable because the processes and products of BB plume processing are dependent on long range transport, cloud processing, varying meteorological conditions and heterogeneous reactions.

In this work we test the ability of CSIRO's high resolution 3D Eulerian grid chemical transport model (CTM) to reproduce BB plume observations of the Robbins Island fire reported in Lawson et al., (2015) with a focus on CO, BC and O_3. We undertake sensitivity studies using varying emission factors associated with a low, medium and high Modified Combustion Efficiency (MCE), which in turn changes the NMOC / NO_x ratio, in contrast to other sensitivity studies which typically ~~vary~~ scale emissions of all species ~~linearly~~by a constant factor (Pacifico

et al., 2015;Lei et al., 2013). We also test sensitivity to meteorology by coupling the CTM with two different meteorological models, TAPM and CCAM. The fire and fixed observation site (Cape Grim) were only 20 km apart, and so simulation of the plume strikes is a stringent test of TAPM and CCAM's ability to reproduce windspeed and direction. Plume rise and chemical mechanism are held constant. Finally, we use TAPM-CTM to separate the contribution of the Robbins Island fire emissions and urban emissions to the observed O_3 enhancements at Cape Grim reported in Lawson et al., (2015), and to determine the age of the O_3-enhanced air parcels.

2 Methods

2.1 Fire and measurement details

Details of the fire and measurements are given in Lawson et al (2015). Briefly, biomass burning (BB) plumes were measured at the Cape Grim Baseline Air Pollution Station during the 2006 Precursors to Particles campaign, when emissions from a fire on nearby Robbins Island impacted the station. Fire burned through native heathland and pasture grass on Robbins Island some 20 km to the east of Cape Grim for two weeks in February 2006. On two occasions an easterly wind advected the BB plume directly to the Cape Grim Station. The first plume strike (BB1) occured from 02:00 – 06:00 (Australian Eastern Standard Time - AEST) on the 16th February, with light easterly winds of 3 m s^{-1} and temperature of 13 ºC and RH of 96 %. The second, more prolonged plume strike (BB2) occurred from 23:00 on 23rd February to 05:00 on the 25th February, with strong easterly winds ranging from 10-16 m s^{-1}, temperatures of 16-22 ºC and RH in the range of 75-95 %. Under a northerly wind direction, urban air from the city of Melbourne (population 4.2 million) some 300 km away is transported across the ocean (Bass Strait) to Cape Grim.

A wide variety of trace gas and aerosol measurements were made during the fire event (Lawson et al., 2015). In this work, measurements of black carbon (BC), carbon monoxide (CO) and ozone (O_3) are compared with model output. BC measurements were made using an aethelometer (Gras, 2007), CO measurements were made using an AGAGE gas chromatography system with a multi-detector (Krummel et al., 2007) and O_3 measurements were made using a TECO analyser (Galbally et al., 2007). For further details see Lawson et al., (2015).

2.2 Chemical transport models

Simulations were undertaken with CSIRO's chemical transport model (CTM), coupled offline with two meteorological models (see below). The CSIRO CTM is a three-dimensional Eulerian chemical transport model with the capability of modelling the emission, transport, chemical transformation, wet and dry deposition of a coupled gas and aerosol phase atmospheric system. The CTM was initially developed for air quality forecasting (Cope et al., 2004) and has had extensive use with shipping emission simulations (Broome et al., 2016), urban air quality (Cope et al., 2014; Galbally et al., 2008), biogenic (Emmerson et al., 2016) and biomass burning studies (Keywood et al., 2015; Meyer et al., 2008; Luhar et al., 2008).

The chemical transformation of gas-phase species was modelled using an extended version of the Carbon Bond 5 mechanism (Sarwar et al., 2008) with updated toluene chemistry (Sarwar et al., 2011). The mechanism was also extended to include the gas phase precursors for secondary (gas and aqueous phase) inorganic and organic aerosols. Secondary inorganic aerosols were assumed to exist in thermodynamic equilibrium with gas phase precursors and were modelled using the ISORROPIA-II model (Fountoukis and Nenes, 2007). Secondary organic aerosol (SOA) was modelled using the Volatility Basis Set (VBS) approach (Donahue et al., 2006). The VBS configuration is similar to that described in Tsimpidi et al., (2010). The production of S-VI in cloud water was modelled using the approach described in Seinfeld and Pandis (1998). The boundary concentrations in the models for different wind directions were informed by Cape Grim observations of atmospheric constituents during non BB periods (Lawson et al., 2015). In this work the modelled elemental carbon (EC) output was considered equivalent to the BC measured with aethalometer at Cape Grim.

Horizontal diffusion is simulated according to equations detailed in Cope et al (2009) according to principles of Smagorinsky et al., (1963) and Hess (1989). Vertical diffusion is simulated according to equations detailed in Cope et al., (2009) according to principles of Draxler and Hess (1997). Horizontal and vertical advection uses the approach of Walcek et al., (2000).

2.2.1 Meteorological models

Prognostic meteorological modelling was used for the prediction of meteorological fields including wind velocity, temperature, water vapour mixing ratio and clouds, radiation and turbulence. The meteorological fields force key components of the emissions and the chemical transport model. Two meteorological models were used in this work. CSIRO's (The) Air Pollution Model (TAPM) (Hurley, 2008b), a limited area, nest-able, three-dimensional

Eulerian numerical weather and air quality prediction system, and CSIRO's Conformal Cubic Atmospheric Model (CCAM) a global stretched grid atmospheric simulation model (McGregor, (2015) and references therein). The models represent two unique (and independent) approaches for generating the meteorological fields required by the chemical transport model.

For CCAM, 20 km spaced simulations over Australia were used by the CTM (with the same grid spacing) to model large scale processes on the continent including the emission and transport of windblown dust, sea salt aerosol and smoke from wildfires. Note that the governing equations for TAPM do not enable this model to simulate spatial scales greater than 1000 km in the horizontal and thus only the CCAM meteorology was available for the continental-scale simulations. TAPM and CCAM 12 km spaced simulations were then used to model the transport of the Melbourne plume to Cape Grim by the CTM (at 12 km grid spacing) with boundary conditions provided by the continental simulation. Nested grid simulations by the CTM at 3 km and 1 km grid spacing utilised TAPM and CCAM meteorology simulated at matching grid spacing. The 1 km spaced meteorological fields were also used to drive a 400 m spaced CTM domain which encompassed Robbin's Island and Cape Grim. This domain was included in the nested grid system because we wanted to better numerically resolve the spatial extent of the fire and the process of plume advection between Robbin's Island and Cape Grim. Figure 1 shows the five nested computational domains used in TAPM-CTM and CCAM-CTM.

In this work the CTM coupled with CCAM meteorological model is referred to as CTM-CCAM, while the CTM coupled with the TAPM meteorological model is referred to as TAPM-CTM.

2.2.2 Emission inventories

Anthropogenic emissions

Anthropogenic emissions for Victoria were based on the work of Delaney et al., (2011). No anthropogenic emissions were included for Tasmania. The north-west section of Tasmania has limited habitation and is mainly farmland, and so the influence of Tasmanian anthropogenic emissions on Cape Grim are expected to be negligible.

Natural and Biogenic emissions

The modelling framework includes methodologies for estimating emissions of sea salt aerosol (Gong, 2003) emissions of windblown dust (Lu and Shao, 1999); gaseous and aerosol

emissions from managed and unmanaged wild fires (Meyer et al., 2008); emissions of NMOC from vegetation (Azzi et al., 2012) and emissions of nitric oxide and ammonia from vegetation and soils. Emissions from all but the wildfires are calculated inline in the CTM at each time step using the current meteorological fields. There were no other major fires burning in Victoria and Tasmania during the study period.

Emissions – Robbins Island fire

The area burnt by the fire was determined from hotspots from the Sentinel product (Geosciences Australia) which were derived from MODIS imagery. The hotspots were buffered to give polygon spots at a resolution of 400ha $spot^{-1}$, then merged into a single polgygon for each fire day (Meyer et al., 2008). ~~T~~ The fire burnt 2000 ha over the two week period, and the direction of fire spread was unknown. As such, the fire scar was divided up into 250m grids and the hourly areas burnt calculated using a normalised version of the Macarthur Fire Danger Index (FDI) (Meyer et al., 2008). The models assumed that an equal proportion of each grid burned simultaneously over the two week period. The fuel density used was estimated to be 18.7 t C ha^{-1}, based on mean mass loads of coarse and fine fuels taken from the biogeochemical production model (VAST 1.2, Barrett 2002) and converted into carbon mass (Meyer et al., 2008).

The hourly diurnal emissions of all gases and particles from the fire were calculated using the FDI in which the presence of strong winds will result in faster fire spread and enhanced emissions, compared to periods of lower wind speeds. The effect of wind speed on the fire behaviour and emissions is particularly important during the second BB event in which the winds ranged from 10 to15 m s^{-1}. This is evident from Figure 2 where hourly emission profiles based on an average diurnal FDI calculated by Meyer et al., (2008) (which peaks early afternoon) is compared with profiles based on hourly FDI generated by TAPM and CCAM meteorology. It can be seen that the use of the dynamic FDI approach during the BB2 period increases the Base emissions by 70% for TAPM meteorology and by 45% for the CCAM meteorology. It is also notable that the use of the dynamic approach with TAPM meteorology leads to the peak emissions occurring overnight on the 24th Feb which is when the Base emissions are at a minimum.

~~Savanna category EF were used as base case EFs in this work from Andreae and Merlet (2001).~~ Three different sets of fire emission factors, corresponding to low, medium and high MCE were used to test the sensitivity of the models, where MCE = ΔCO_2 / ΔCO + ΔCO_2 (Ferek et

al., 1998). We used published EF of CO and CO_2 from temperate forests (Akagi et al., 2011), to calculate a typical range of MCEs for temperate fires, including an average (best estimate) of 0.92, a lower (0.89) and upper estimate (0.95). Fires with MCEs of approximately 0.90 consume biomass with approximately equal amounts of smouldering and flaming, while MCEs of 0.99 indicate complete flaming combustion (Akagi et al., 2011). Therefore the calculated range of MCEs (0.89 - 0.95) correspond to fires in which both smouldering and flaming is occurring, with a tendency for more flaming combustion in the upper estimate (0.95) compared to a tendency of more smouldering in the lower estimate (0.89).

In previous smoke modelling work, CCAM-CTM and TAPM-CTM used savannah EF from Andreae and Merlet (2001). However, as Robbins Island is in a temperate region, the Andreae and Merlet (2001) savannah EF used in the models were adjusted to reflect temperate EF based on the following methodology. Minimum, mean and maximum CO EF for temperate forests from Agaki et al., (2011) were used for lower ~~(0.89)~~, best estimate ~~(0.92)~~ and upper MCE ~~(0.95)~~. For all other species, savannah EF (corresponding to MCE 0.94) were adjusted to EF for the lower, best estimate and upper MCE~~s=0.89, 0.92 and 0.95~~ using published relationships between MCE and EF (Meyer et al., 2012; Yokelson et al., 2007; Yokelson et al., 2003; Yokelson et al., 2011).

For example to adjust the Andreae and Merlet (2001) savannah EF (corresponding to an MCE of 0.94) to our temperate 'best estimate' EF (corresponding to MCE of 0.92) the Andreae and Merlet (2001) NO EF was reduced by 30%, the NMOC EFs were increased by 30%, the BC EF was reduced by 30% and the OC EF was increased by 20%. Table 1 gives emission factors for the original savannah EF (Andreae and Merlet, 2001) and the adjusted EF used in this work. The NO_x/NMOC ratios used are also shown, and vary by a factor of 3 between the low and high MCE scenarios, mainly driven by the variability in NO emissions with MCE. The EF calculated from observations for this fire are shown for comparison (Lawson et al., 2015).

We recognise calculating EF in this way is approximate, however the purpose of including a range of EF was to explore the model's sensitivity to EF. While EFs were calculated for the Robbins Island fire for several species (Lawson et al., 2015), these are only available for a subset of species required by the CB05 chemical mechanism. The adjustment of the Andreae and Merlet (2001) Savannah EF to a lower MCE (0.89) resulted in good (± 20%) agreement with the calculated EF for CO, BC and several NMOC from Lawson et al., (2015), in which the MCE was calculated as 0.88. This provides confidence in using published relationships between MCE and EF to estimate EF in this work.

With respect to plume rise, the Robbin's Island fire was a relatively low energy burn (Lawson et al., 2015), and as noted by Paugam et al., (2016) the smoke from such fires is largely contained within the planetary boundary layer (PBL). Given that ground-based images of the Robbin's Island smoke plume support this hypothesis, in this work we adopted a simple approach of mixing the emitted smoke uniformly into the model's layers contained within the PBL. The plume was well mixed between the maximum of the PBL height and 200 m above the ground, with the latter included to account for some vertical mixing of the buoyant smoke plume even under conditions of very low PBL height. The high wind speeds particularly during the second BB event, also suggest that the plume was not likely to be sufficiently buoyant to penetrate the PBL.

3 Results and Discussion

3.1 Modelling Sensitivity Study

The ability of the models to reproduce the two plume strikes (BB1 and BB2, described in Lawson et al (2015)) was tested. The period examined was the 13 February 2006 to the 28 February 2006. The sensitivity of the models to meteorology, emission factors and spatial variability was also investigated and is discussed below. Observation and model data shown are hourly averages. Table 2 summarizes the main findings of the model sensitivity study. A MODIS Truecolour Aqua image of the Robbins Island fire plume is shown in Figure 3 from 23 February 2006, with the modelled plume during the same period.

3.1.1 Sensitivity of modelled BB species to meteorology

Qualitative and quantitative assessment of model performance for meteorological parameters were undertaken for both TAPM and CCAM. Hourly observed and modelled winds, temperature, humidity and PBL are compared and discussed in the Supplementary section (Figures S2-S8). Briefly, both TAPM and CCAM demonstrated reasonable skill in modelling the meteorological conditions, with the TAPM simulations slightly better than the CCAM with respect to the low level wind, temperatures and relative humidity and CCAM simulations slightly better in terms of PBL height.

Primary species- CO and BC

Figure 4 and Figure 5 show concentration isopleths for BC generated by TAPM-CTM and CCAM-CTM for BB1 and BB2 respectively. The simulated and observed time series concentrations of CO and BC for the two different models (TAPM-CTM and CCAM-CTM) and for 3 different sets of EF (discussed in Section 3.1.2) are shown in Figure 6. TAPM-CTM and CCAM-CTM both reproduce the observed plume strikes (BB1 and BB2). The impact of meteorology on the plume strike timing and duration is discussed below.

Both models overestimate the duration of BB1 and are a few hours out in the timing of the plume strike. TAPM-CTM predicts the timing of BB1 is 3 hours later than occurred (BC data) and predicts that BB1persists for 12 hours (observed duration 5 hours). CCAM-CTM predicts that BB1 occurs 12 hours prior to the observed plume strike and predicts that the plume intermittently sweeps across Cape Grim for up to 36 hours (Figure 4). Both models indicate that the plume is narrow and meandering.

Both models overestimate the duration of BB2 and simulate the plume strike occurring earlier than observed. TAPM-CTM predicts BB2 is 26 hours earlier than observed and that BB2 persists for 50 hours (observed duration 29 hours). CCAM-CTM predicts BB2 is 26 hours earlier than observed and that BB2 persists for 57 hours. It should be noted that there is a brief observed enhancement of BB species which correspond with the beginning of the modelled BB2 plume strike, some 24 hours prior to the prolonged observed event. This was likely due to the edge of the plume impacting the station briefly.

In both observed BB1 and BB2 the plume strike at Cape Grim occurred just prior to a wind direction change from easterly (fire direction), to south-westerly. The timing of the wind direction change in the models is therefore crucial to correctly predicting plume strike time and duration. In BB1 CCAM predicts an earlier wind direction change with higher windspeeds which advects the plume directly over Cape Grim while TAPM predicts a later wind change, lower windspeeds and advection of only the edge of the plume over Cape Grim. The higher concentrations CO and BC in BB1 by CCAM-CTM is are likely due to the direct advection of the plume over the site compared to only the plume edge in TAPM-CTM.

In BB2, both TAPM-CTM and CCAM-CTM predict direct strikes of the Robbin's Island smoke plume on Cape Grim, because the wind direction is modelled to be predominantly easterly for the duration of the event (Figure 5~~Fig S18~~). Both models simulate some backing and veering of the wind direction for the duration of BB2 due to gravity waves processes which

lead to intermittent strikes on Cape Grim as the Robbin's Island smoke plume sweeps to the north and south of Cape Grim. The gravity wave oscillations are more pronounced in CCAM-CTM than TAPM-CTM (and thus the plume strikes are more pronounced from the former) due to differences in how the models are coupled to large scale synoptic forcing. The event is eventually curtailed by the passage of a south-westerly change.

Figure 5~~Fig. S18~~ shows that TAPM-CTM predicts the onset of the change to occur about six hours ahead of the observed change and thus the BB2 event ends too early for this meteorological simulation. CCAM-CTM models the south-westerly change to occur one hour after the observed, leading to the modelled BB2 event extending beyond the observed duration for this meteorological simulation.

Differences in the magnitude of the modelled CO and BC peaks for TAPM-CTM and CCAM-CTM have two principal cause: a), the coupling of the smoke emissions to the TAPM and CCAM meteorology via the FDI scaling leads to approximately 20% higher emissions in the case of the TAPM-CTM simulations; b), the CCAM wind speeds are 20-50% higher than the TAPM wind speeds during BB2, which in combination with the emission differences, leads to TAPM-CTM generating near-surface smoke concentrations which are up to 80% higher than CCAM-CTM. Mixing depth can also play an important role in plume dispersion, however the PBL heights generated by both models are similar and generally low during BB2 due to the easterly wind direction and the mainly maritime upwind fetch.

Secondary species – O_3

Figure 6 e-f shows the simulated and actual O_3 concentration time series for TAPM-CTM and CCAM-CTM for 3 different sets of EF (discussed in Section 3.1.2). The two observed O_3 peaks which followed BB1 and BB2 can clearly be seen in the time series of observations. Figure 7~~Figure 7~~ shows the TAPM-CTM and CCAM-CTM concentration isopleths of O_3 enhancement downwind of the fire during BB1 at 11:00 and 13:00 on the 16 February.

Again the simulated meteorology has a major impact on the ability of the models to reproduce the magnitude and timing of the observed O_3 peaks. TAPM-CTM reproduces the major O_3 peak observed following BB2, and captures part of the O_3 peak following BB1. For the peak following BB1 it under predicts the peak duration and fails to capture the subsequent observed peaks on the 19th and 19th February. TAPM-CTM also shows 2 additional O_3 peaks about 24 hours prior to the BB1 and BB2 peaks respectively, which were not observed. The magnitude of these additional peaks shows a strong dependency on the EF suggesting an

influence of fire emissions. This is discussed further below and in Section 3.2.1.Compared to TAPM-CTM, CCAM-CTM predicts fewer distinct peaks of ozone above the background (where background is 15-17 ppb) throughout the entire period. Both TAPM-CTM and CCAM-CTM show depletion of O_3 below background levels which was not observed, and this is discussed further in Section 3.1.2.

Figure 7~~Figure 7~~ shows that there are differences in wind fields between TAPM-CTM and CCAM-CTM as well as different simulated concentrations of O_3 generated from the fire. This is discussed further in Section 3.1.2. To summarise, the impact of using two different meteorological models for a primary species such as BC was to vary the modelled time of impact of the BB1 plume strike by up to 15 hours (CCAM-CTM -12 and TAPM-CTM +3 hours, where actual plume strike time = 0 hours) and to vary the plume duration between 12 and 36 hours (actual duration 5 hours). For BB2, different meteorological models predicted the same impact time (TAPM-CTM and CCAM-CTM both -26 hours where actual plume strike time = 0 hours and to vary the plume duration between 47 and 60 hours (actual duration 29 hours).

For O_3, the use of different meteorological models lead to one model (TAPM-CTM) reproducing both observed peaks plus two additional peaks, while the other model (CCAM-CTM) captured only one defined O_3 peak over the time series of 2 weeks.

3.1.2 Sensitivity of modelled BB species to Emission Factors

Primary species – CO and BC

Figure 6 a-d shows the simulated and observed concentrations of BC and CO for MCE=0.89, MCE=0.92 and MCE=0.95 (see Section 2.2.2). Because CO has a negative relationship with MCE, and BC has a positive relationship with MCE, the modelled BC concentrations are highest for model runs using the highest MCE, while the modelled CO concentrations are highest for model runs using the lowest MCE (Figure 6).

Changing the EF from low to high MCE varies the modelled BC concentrations during BB1 and BB2 by a factor of ~3 for BC and a factor of ~2 for CO, and increases the EF ratio of BC/CO by a factor of ~6, in proportion to the difference in EF input to the models.

Quantile-quantile plots of observed and modelled ratios of BC/CO during BB1 and BB2 for the different EF scenarios are shown in Figure 8~~Fig S11~~. The use of BC/CO ratios were used to minimise uncertainty resulting from errors in modelling transport, dilution (and mixing

height), thus enabling a focus on the impact of EF variability. A period incorporating both the modelled and observed BB1 and BB2 was used for the analysis. The TAPM-CTM simulation with MCE=0.89 performed best with greater than 60% of the model percentiles falling within a factor of two of the observed. The CCAM-CTM simulation with MCE = 0.89 was the second best performer with 50% of the modelled percentiles falling within a factor of two of the observed. Overestimates of the EC/CO ratio by up to a factor of 8 occur for some percentiles for the MCE=0.95 scenarios, while the scenarios with no fire significantly underestimated the observed ratio. Plots of mean fractional bias and mean fractional error (Fig. S12~~2~~1 and S12~~3~~) show that TAPM-CTM simulation with MCE=0.89 has the smallest bias and error, followed by the CCAM-CTM simulation with MCE=0.89. As discussed previously there is uncertainty in the derivation of EF as a function of MCE, as these were based on relationships from a small number of studies. Nevertheless, the percentile, bias and error analysis indicates that using emission factors corresponding to an MCE of 0.89 gives the best agreement with the observations for the BC/CO ratio. This is in agreement with the calculated MCE of 0.88 for this fire (Lawson et al., 2015)

Secondary species - O_3

For secondary species such as O_3 (Figure 6e-f), the relationship between EF precursor gases and model output is more complex than for primary species such as CO and BC, because the balance between O_3 formation and destruction is dependent on the degree of dilution of the BB emissions and also factors such as the NMOC composition and the NMOC/NO_x ratio.

TAPM-CTM (Figure 6e) reproduces the magnitude of both observed peaks following BB1 and BB2 (BB1 max observed = 33 ppb, modelled = 31 ppb, BB2 max observed = 34 ppb, modelled = 30ppb). Interestingly the magnitude of O_3 for these two peaks is the same for different EF inputs of O_3 precursors from the Robbins Island fire, suggesting that the BB emissions are not responsible for these enhancements as demonstrated in Section 3.2. In contrast, the two additional peaks modelled but not seen in the observations are heavily dependent on the input EF. For the first additional modelled peak which was predicted at the time of BB1observations on the 16th February, all EF scenarios result in an O_3 peak, with the MCE=0.92 model scenario resulting in highest predicted O_3. For the second additional modelled peak just prior to the BB2 observations on the 23rd February, only the MCE=0.89

scenario results in a net O_3 production, while MCE=0.92 and MCE=0.95 scenarios lead to net O_3 destruction.

This differing response to EF for the TAPM-CTM runs suggests the importance of the NO EF on O_3 production in BB plumes. Unfortunately there were no oxides of nitrogen measurements made during the fire to test the models. For the first simulated additional peak prior to BB1, while the medium NO EF (MCE=0.92) resulted in the highest O_3 peak (with corresponding NO of 3.7 ppb, NO_2 4.5 ppb) the lower NO EF in the 0.89 MCE run perhaps indicates insufficient NO was present to drive O_3 production (corresponding NO 0.5 ppb, NO_2 1.5 ppb), which is in line with studies which have shown that BB plumes are generally NO_x limited (Akagi et al., 2013; Jaffe and Wigder, 2012; Wigder et al., 2013). Conversely the highest input NO EF (MCE=0.95) lead to net destruction of O_3 (NO 9 ppb, NO_2 7 ppb), which is due to titration of O_3 with the larger amounts of NO emitted from the fire in these runs as indicated by excess NO (NO/NO_2 ratio > 1) at Cape Grim (where NO has a positive relationship with MCE). For the second additional peak prior to BB2, only the lowest NO EF run (MCE=0.89) resulted in net production of O_3 (NO 1.5 ppb NO_2 2.6 ppb) in the medium and high MCE runs the background O_3 concentration is completely titrated (0 ppb) with NO concentrations of 10 and 20 ppb and NO/NO_2 ratios of 1.3 and 2.6 respectively.

In contrast, the CCAM-CTM model (Figure 6f) simulations reproduce only the first observed O_3 peak associated with BB1 (modelled = 27 ppb, measured = 34 ppb). This modelled O_3 peak does not show an influence of MCE on O_3 concentration, in agreement with TAPM, again suggesting no influence from fire emissions as later demonstrated in Section 3.2. The CCAM model runs also show significant titration of O_3 during BB1 and BB2 for the medium and high MCE model runs, with ~24 and ~48 hours of significant O_3 depletion below background concentrations being modelled for each event, which was not observed

Quantile-quantile plots of modelled and observed concentrations of O_3 for all EF scenarios are shown in Figure 9~~Figure 8Fig. S14~~ and S1~~3~~5. Model performance was assessed for both the BB and the background periods in order to test the ability of the models to reproduce O_3 from both the fire and other sources, including urban sources. The modelled O_3 concentrations from the TAPM-CTM simulation with MCE=0.89 are close to the 1:1 line with observations for all of the sampled percentiles, and demonstrates that this scenario is in best agreement with observations, and as stated previously, in agreement with the calculated MCE of 0.88 for BB2 (Lawson et al., 2015). Ozone titration in the MCE=0.92 and MCE=0.95 scenarios, which was not observed, is visible as a significant deviation from the 1:1 line in Figure 9~~Fig S14~~. With

the exception of these titration events, all of the sampled model concentration percentiles fall well within a factor of two of the observations. Plots of mean fractional error and mean fractional bias (Figs S146 and S157) show that the error and bias are very low for all runs and fall within performance guidelines.

The different EF scenarios presented here suggest that varying model EF has a major impact on whether the models simulate production or destruction of O_3, particularly important at a receptor site in close proximity to the BB emissions. In the previous work (Lawson et al., 2015), the MCE for the first 10 hours of BB2 was calculated as 0.88, however later in BB2, a rainfall event led to changes in the NMOC/CO and BC/CO ratios. This suggests that during the course of BB2 the MCE decreased and thus EFs changed. As such, the used of fixed BB EF in this work and in other models, may lead to incorrect prediction of important species such as O_3.".

3.1.3 Sensitivity of modelled concentrations to spatial variability

The near-field proximity of the Robbins Island fire (20 km) to Cape Grim, the narrowness of the BB plume and the spatial complexity of the modelled wind fields around north Tasmania are likely to result in strong heterogeneity in the modelled concentrations surrounding Cape Grim. We investigated how much model spatial gradients vary by sampling TAPM-CTM output with MCE=0.89 at 4 grid points sited 1 km to the north, east, south and west of Cape Grim.

Primary species - CO

Figure 10a shows a time series of the modelled CO output of the difference between Cape Grim and each grid point 1km either side.

Where plotted CO concentration is other location [CO] (N,S,E,W) –Cape Grim [CO].

The figure clearly shows that there are some large differences in the modelled concentrations of CO between grid points for both BB1 and BB2. Particularly large differences were seen for BB2 with the north gridpoint modelled concentrations in BB2 over 500 ppb lower than at Cape Grim grid point, while at the Southerly grid point the modelled CO was up to 350 ppb higher. Smaller differences of up to 250 ppb between the east and Cape Grim grid points were observed for BB1. This indicates the plume from the fire was narrow and had a highly variably impact on the area immediately surrounding Cape Grim.

Figure 10Figure 8b shows the observed cumulative concentration of CO over the 29 hour duration of BB2 at Cape Grim, as well as the modelled cumulative concentration at Cape Grim

and at the four gridpoints either side. This figure shows both the variability in concentration with location, but also with time. TAPM-CTM's underestimation of the observed CO by is visible by hour 20. TAPM-CTM begins to show differences in modelled cumulative CO concentrations between the 5 gridpoints (including Cape Grim) by hour 10. At the end of BB2 TAPM-CTM predicts that there are differences of 5 - 30% between the cumulative modelled CO concentration at Cape Grim and the gridpoints to the north, east, south and west. his variability modelled between sites which are closely located highlights the challenges with modelling the impact of a near field fire at a fixed single point location. This also highlights the high spatial variability which may be missed in similar situations by using a coarser resolution model which would dilute emissions in a larger gridbox.

Ozone (O_3)

Figure 10~~Figure 8~~c shows a time series of the modelled O_3 output of the difference between Cape Grim and each gridpoint 1km either side, where plotted O_3 concentration is other location $[O_3]$ (N,S,E,W) – Cape Grim $[O_3]$.

The modelled TAPM-CTM concentrations are very similar at all grid points when BB emissions are not impacting. The variability increases at the time of BB1 and BB2, with differences mostly within 2-3 ppb, but up to 15 and 10 ppb at east and west sites for BB1. This largest difference corresponds to the additional modelled O_3 peak which was not observed which showed strong dependency on EF (see Section 3.1.2), and provides further evidence that local BB emissions are driving this enhancement.

The TAPM-CTM output for O_3 for BB1(Figure 7~~Figure 7~~) shows O_3 enhancement downwind of the fire at 11:00 and 13:00 on the 16 February. The very localised and narrow O_3 plume is dispersed by the light (2 m s^{-1}) and variable winds, and Cape Grim is on the edge of the O_3 plume for much of this period, explaining the high variability seen in Figure 6c.

In summary there is a large amount of spatial variability in TAPM-CTM for primary species such as CO during the BB events, with differences of > 500 ppb in grid points 1 km apart. This is due to the close proximity of the fire to the observation site and narrow plume non-stationary meteorology. For O_3, there is up to 15 ppb difference between grid points for a narrow O_3 plume which is formed downwind of the fire.

The highly localised nature of the primary and in some cases secondary species seen here highlights the benefits of assessing spatial variability in situations with a close proximity point source and a fixed receptor (measurement) site.

3.2 Exploring plume chemistry and contribution from different sources

3.2.1 Drivers of O_3 production

In previous work on the Robbins Island fire, it was noted that the increases in O_3 observed after both BB1 and BB2 were correlated with increased concentration of HFC134a (Lawson et al., 2015). This indicated that transport of photochemically processed air from urban areas to Cape Grim was likely the main driver of the O_3 observed, rather than BB emissions (Lawson et al., 2015). However, during BB1 in a calm sunny period with minimal urban influence, an increase in O_3 was observed alongside a period of particle growth and elevated BC, suggesting possible biomass burning influnce. Normalised Excess Mixing Ratios (NEMR) observed during BB2 were also in the range of those observed elsewhere in young BB plumes (Lawson et al., 2015) (where NEMR is an excess mixing ratio normalised to a non-reactive co-emitted tracer, in this case CO, see Akagi et al., 2011).

To explore this further, TAPM-CTM was used to determine the degree to which the local fire emissions, and urban emissions from mainland Australia, were driving the observed O_3 enhancements. The scenario with EF corresponding to MCE=0.89 was used, as discussed previously

Figure 11~~Figure 9~~ shows the simulated ozone for all sources (With BB) and all sources excluding the Robbins Island fire (No BB). There are two additional distinct ozone peaks in the 'With BB' simulation (Figure 11~~Figure 9~~). These occured during, or close to the plume strikes, and are short lived (3 and 5 hour) events. These same two peaks showed a strong dependance on model EF in Section 3.1.2. In contrast, the two peaks attributed to transport of air from mainland Australia are of longer duration, and occur after the plume strikes.

Of the 2 modelled fire-derived O_3 peaks, the first modelled peak (33 ppb) corresponds with a small (21 ppb) observed peak during BB1 (Period B in Lawson et al., 2015), but the second modelled fire-derived O_3 peak is not observed. As shown in Figure 7~~Figure 7~~ and discussed in Section 3.1.3, according to TAPM-CTM the O_3 plumes generated from fire emissions were narrow and showed a strong spatial variability. Given this, it is challenging for TAPM-CTM to predict the exact timing and magnitude of these highly variable BB generated O_3 peaks impacting Cape Grim. This is likely why there is good agreement in timing and magnitude between model and observations for the large scale, spatially homogeneous O_3 plumes transported from mainland Australia, but a lesser agreement for the locally formed, spatially variable O_3 formed from local fire emissions.

In summary, TAPM-CTM suggests that the the two largest observed O_3 peaks followng BB1 and BB2 were urban air transported from mainland Australia, and suggests some O_3 formation was driven by emissions from the local fire event. TAPM-CTM captures the magnitude and timing of the larger scale urban-derived peaks well, but is challenged by the timing and magnitude of O_3 from local BB emissions.

3.2.2 Plume age

TAPM-CTM was used to estimate the physical age of air parcels reaching Cape Grim over the two week period of the Robbins Island fire. The method is similar to the Eulerian effective physical age of emissions metric, accounting for mixing and chemical decay from Finch et al (2014) and has been described previously in Keywood et al., (2015). Briefly, two model simulations were run for scenarios which included all sources of nitric oxide (NO) in Australia; the first treated NO as an unreactive tracer, the second with NO decaying at a constant first order rate. The relative fraction of the emitted NO molecules remaining after 96 hours was then inverted to give a molar-weighted plume age. As urban emissions are a larger NO source than BB, this approach would weight the age in the favour of the urban emissions if air masses from these two sources were mixed. However as shown in Figure 11~~Figure 9~~, there are distinct periods where BB or urban sources dominate. As there is little mixing of air from the two sources, there are unlikely to be issues with the calculated age being weighted towards one source. Figure 12~~Figure 10~~ shows a time series of the modelled NO tracer (decayed version), modelled plume age (hours) and the observed O_3. Direct BB1 and BB2 plume strikes can be clearly seen with increases in NO corresponding with a plume age of 0-2 hours. The plume age then gradually increases over 24 hours in both cases, peaking at 15:00 on the 17th February during BB1 (aged of plume 40 hours) and peaking at 17:00 on the 25th February during BB2 (age of plume 49 hours). The peak observed O_3 enhancements correspond with the simulated plume age in both BB1 and BB2 (with an offset of 2 hours for BB1), and the observed HFC-134a, suggesting that the plume which transported O_3 from Mebourne to Cape Grim was approximately 2 days old. TAPM-CTM also simulates a smaller NO peak alongside the maximum plume age, indicating transport of decayed NO from the mainland to Cape Grim.

As reported in Lawson et al., (2015), during BB2 NEMRs of $\Delta O_3/\Delta CO$ ranged from 0.001-0.074, in agreement with O_3 enhancements observed in young BB plumes elsewhere (Yokelson et al., 2003; Yokelson et al., 2009). However, the modelling reported here suggests that almost

all of the O_3 observed during BB2 was of urban, not BB origin. This suggests NEMRs should not be used in isolation to identify the source of observed O_3 enhancements, and highlights the value of utilising air mass back trajectories and modelling to interpret the source of O_3 enhancements where there are multiple emission sources.

4 Summary and conclusions

In this work we have used a unique set of opportunistic BB observations at Cape Grim Baseline Air Pollution Station to test the ability of CSIRO's high resolution (400m grid cell) CTM to reproduce primary (CO, BC) and secondary (O_3) BB species in challenging non-stationary, inhomogeneous, and near field conditions. We tested the sensitivity of the CTM to three different parameters (meteorology, MCE and spatial variability) while holding the plume rise and the chemical mechanisms constant.

We found meteorology, EF and spatial variability have a large influence on the modelled output mainly due to the close proximity of the fire to the receptor site (Cape Grim). The lower MCE (MCE=0.89) TAPM-CTM model simulation provided the best agreement with the observed concentrations, in agreement with the MCE calculated from observations of 0.88 (Lawson et al., 2015). The changing EFs, in particular NO dependency on MCE, had a major influence on the simulated O_3 concentrations, with a tendency of the models in some configurations to both fail to simulate observed O_3 peaks, and to simulate complete titration of O_3 which was not observed. As shown in the previous work (Lawson et al., 2015), minor rainfall events have the potential to significantly alter EF due to changes in combustion processes. This work suggests that varying model EF has a major impact on whether the models predict production or destruction of O_3, particularly important at a receptor site in close proximity to the BB emissions. Models which assume a fixed EF for O_3 precursor species in an environment with temporally and spatially variable EF may therefore be challenged to correctly predict the behaviour of important species such as O_3.

There were significant differences in model output between Cape Grim and grid points 1 km away highlighting the narrowness of the plume and the challenge of predicting when the plume would impact the station. This also highlights the high spatial variability which may be missed in similar situations by using a coarser resolution model which would dilute emissions in a larger gridbox.

TAPM-CTM was used to distinguish the influence of the two sources on the observed O_3 enhancements which followed BB1 and BB2. Transport of a 2 day old urban plume some

300km away from Melbourne was the main source of the O_3 enhancement observed at Cape Grim over the two week period of the fire. Despite NEMRs of $\Delta O_3/\Delta CO$ during BB2 being similar to that observed in young BB plumes elsewhere, this work suggests NEMRs should not be used in isolation to identify the source of observed O_3 enhancements, and highlights the value of utilising air mass back trajectories and modelling to interpret the source of O_3 enhancements where there are multiple emission sources.

Acknowledgements

The Cape Grim program, established by the Australian Government to monitor and study global atmospheric composition, is a joint responsibility of the Bureau of Meteorology (BOM) and the Commonwealth Scientific and Industrial Research Organisation (CSIRO). We thank the staff at Cape Grim and staff at CSIRO Oceans and Atmosphere for providing observation data for this work. Thank you to Nada Derek for producing figures, Mick Meyer for providing fire scar information, and Suzie Molloy for providing advice on ozone observation data. Finally we thank the three anonymous reviewers for their helpful suggestions and comments

References

Akagi, S. K., Yokelson, R. J., Wiedinmyer, C., Alvarado, M. J., Reid, J. S., Karl, T., Crounse, J. D., and Wennberg, P. O.: Emission factors for open and domestic biomass burning for use in atmospheric models, Atmospheric Chemistry and Physics, 11, 4039-4072, 10.5194/acp-11-4039-2011, 2011.

Akagi, S. K., Yokelson, R. J., Burling, I. R., Meinardi, S., Simpson, I., Blake, D. R., McMeeking, G. R., Sullivan, A., Lee, T., Kreidenweis, S., Urbanski, S., Reardon, J., Griffith, D. W. T., Johnson, T. J., and Weise, D. R.: Measurements of reactive trace gases and variable O3 formation rates in some South Carolina biomass burning plumes, Atmos. Chem. Phys., 13, 1141-1165, 10.5194/acp-13-1141-2013, 2013.

Alvarado, M. J., and Prinn, R. G.: Formation of ozone and growth of aerosols in young smoke plumes from biomass burning: 1. Lagrangian parcel studies, Journal of Geophysical Research, 114, 10.1029/2008jd011144, 2009.

Alvarado, M. J., Wang, C., and Prinn, R. G.: Formation of ozone and growth of aerosols in young smoke plumes from biomass burning: 2. Three-dimensional Eulerian studies, Journal of Geophysical Research, 114, 10.1029/2008jd011186, 2009.

Alvarado, M. J., Lonsdale, C. R., Yokelson, R. J., Akagi, S. K., Coe, H., Craven, J. S., Fischer, E. V., McMeeking, G. R., Seinfeld, J. H., Soni, T., Taylor, J. W., Weise, D. R., and Wold, C. E.: Investigating the links between ozone and organic aerosol chemistry in

a biomass burning plume from a prescribed fire in California chaparral, Atmos. Chem. Phys., 15, 6667-6688, 10.5194/acp-15-6667-2015, 2015.

Anderson, D. C., Nicely, J. M., Salawitch, R. J., Canty, T. P., Dickerson, R. R., Hanisco, T. F., Wolfe, G. M., Apel, E. C., Atlas, E., Bannan, T., Bauguitte, S., Blake, N. J., Bresch, J. F., Campos, T. L., Carpenter, L. J., Cohen, M. D., Evans, M., Fernandez, R. P., Kahn, B. H., Kinnison, D. E., Hall, S. R., Harris, N. R., Hornbrook, R. S., Lamarque, J. F., Le Breton, M., Lee, J. D., Percival, C., Pfister, L., Pierce, R. B., Riemer, D. D., Saiz-Lopez, A., Stunder, B. J., Thompson, A. M., Ullmann, K., Vaughan, A., and Weinheimer, A. J.: A pervasive role for biomass burning in tropical high ozone/low water structures, Nature communications, 7, 10267, 10.1038/ncomms10267, 2016.

Andreae, M. O., and Merlet, P.: Emission of trace gases and aerosols from biomass burning, Global Biogeochemical Cycles, 15, 955-966, 10.1029/2000gb001382, 2001.

Andreae, M. O., Artaxo, P., Brandao, C., Carswell, F. E., Ciccioli, P., da Costa, A. L., Culf, A. D., Esteves, J. L., Gash, J. H. C., Grace, J., Kabat, P., Lelieveld, J., Malhi, Y., Manzi, A. O., Meixner, F. X., Nobre, A. D., Nobre, C., Ruivo, M., Silva-Dias, M. A., Stefani, P., Valentini, R., von Jouanne, J., and Waterloo, M. J.: Biogeochemical cycling of carbon, water, energy, trace gases, and aerosols in Amazonia: The LBA-EUSTACH experiments, Journal of Geophysical Research-Atmospheres, 107, 8066 10.1029/2001jd000524, 2002.

Arnold, S. R., Emmons, L. K., Monks, S. A., Law, K. S., Ridley, D. A., Turquety, S., Tilmes, S., Thomas, J. L., Bouarar, I., Flemming, J., Huijnen, V., Mao, J., Duncan, B. N., Steenrod, S., Yoshida, Y., Langner, J., and Long, Y.: Biomass burning influence on high-latitude tropospheric ozone and reactive nitrogen in summer 2008: a multi-model analysis based on POLMIP simulations, Atmospheric Chemistry and Physics, 15, 6047-6068, 10.5194/acp-15-6047-2015, 2015.

Artaxo, P., Rizzo, L. V., Brito, J. F., Barbosa, H. M. J., Arana, A., Sena, E. T., Cirino, G. G., Bastos, W., Martin, S. T., and Andreae, M. O.: Atmospheric aerosols in Amazonia and land use change: from natural biogenic to biomass burning conditions, Faraday Discuss., 165, 203-235, 10.1039/c3fd00052d, 2013.

Azzi, M., Cope, M., and Rae, M.: Sustainable Energy Deployment within the Greater Metropolitan Region. NSW- Environmental Trust 2012.

Barrett, D. J.: Steady state turnover time of carbon in the Australian terrestrial biosphere, Global Biogeochemical Cycles, 16, 55-51-55-21, 10.1029/2002gb001860, 2002.

Broome, R. A., Cope, M. E., Goldsworthy, B., Goldsworthy, L., Emmerson, K., Jegasothy, E., and Morgan, G. G.: The mortality effect of ship-related fine particulate matter in the Sydney greater metropolitan region of NSW, Australia, Environment International, 87, 85-93, http://dx.doi.org/10.1016/j.envint.2015.11.012, 2016.

Castellanos, P., Boersma, K. F., and van der Werf, G. R.: Satellite observations indicate substantial spatiotemporal variability in biomass burning NOx emission factors for South America, Atmospheric Chemistry and Physics, 14, 3929-3943, 10.5194/acp-14-3929-2014, 2014.

Cope, M., Lee, S., Noonan, J., Lilley, B., Hess, G. D., and Azzi, M.: Chemical Transport Model - Technical Description, 2009.

Cope, M., Keywood, M., Emmerson, K., Galbally, I. E., Boast, K., Chambers, S., Cheng, M., Crumeyrolle, S., Dunne, E., Fedele, R., Gillett, R., Griffiths, A., Harnwell, J., Katzfey,

J., Hess, D., Lawson, S. J., Miljevic, B., Molloy, S., Powell, J., Reisen, F., Ristovski, Z., Selleck, P., Ward, J., Zhang, C., and Zeng, J.: Sydney Particle Study Stage II., 2014. http://141.243.32.146/resources/aqms/SydParticleStudy10-13.pdf

Cope, M. E., Hess, G. D., Lee, S., Tory, K., Azzi, M., Carras, J., Lilley, W., Manins, P. C., Nelson, P., Ng, L., Puri, K., Wong, N., Walsh, S., and Young, M.: The Australian Air Quality Forecasting System. Part I: Project Description and Early Outcomes, Journal of Applied Meteorology, 43, 649-662, doi:10.1175/2093.1, 2004.

Delaney, W., and Marshall, A. G.: Victorian Air Emissions Inventory for 2006, 20th International Clean Air and Environment Conference, Auckland,, 2011.

Dennekamp, M., Straney, L. D., Erbas, B., Abramson, M. J., Keywood, M., Smith, K., Sim, M. R., Glass, D. C., Del Monaco, A., Haikerwal, A., and Tonkin, A. M.: Forest Fire Smoke Exposures and Out-of-Hospital Cardiac Arrests in Melbourne, Australia: A Case-Crossover Study, Environmental health perspectives, 123, 959-964, 10.1289/ehp.1408436, 2015.

Donahue, N. M., Robinson, A. L., Stanier, C. O., and Pandis, S. N.: Coupled Partitioning, Dilution, and Chemical Aging of Semivolatile Organics, Environmental Science & Technology, 40, 2635-2643, 10.1021/es052297c, 2006.

Draxler, R.R and Hess, G.D. .: Description of the HYSPLIT_4 modeling system. NOAA Technical Memorandum ERL ARL-224, Air Resources Laboratory Silver Spring, Maryland, USA, 1997.

Emmerson, K. M., Galbally, I. E., Guenther, A. B., Paton-Walsh, C., Guerette, E. A., Cope, M. E., Keywood, M. D., Lawson, S. J., Molloy, S. B., Dunne, E., Thatcher, M., Karl, T., and Maleknia, S. D.: Current estimates of biogenic emissions from eucalypts uncertain for southeast Australia, Atmos. Chem. Phys., 16, 6997-7011, 10.5194/acp-16-6997-2016, 2016.

Emmons, L. K., Apel, E. C., Lamarque, J. F., Hess, P. G., Avery, M., Blake, D., Brune, W., Campos, T., Crawford, J., DeCarlo, P. F., Hall, S., Heikes, B., Holloway, J., Jimenez, J. L., Knapp, D. J., Kok, G., Mena-Carrasco, M., Olson, J., O'Sullivan, D., Sachse, G., Walega, J., Weibring, P., Weinheimer, A., and Wiedinmyer, C.: Impact of Mexico City emissions on regional air quality from MOZART-4 simulations, Atmospheric Chemistry and Physics, 10, 6195-6212, 10.5194/acp-10-6195-2010, 2010.

Finch, D. P., Palmer, P. I., and Parrington, M.: Origin, variability and age of biomass burning plumes intercepted during BORTAS-B, Atmos. Chem. Phys., 14, 13789-13800, 10.5194/acp-14-13789-2014, 2014.

Ferek, R. J., Reid, J. S., Hobbs, P. V., Blake, D. R., and Liousse, C.: Emission factors of hydrocarbons, halocarbons, trace gases and particles from biomass burning in Brazil, Journal of Geophysical Research: Atmospheres, 103, 32107-32118, 10.1029/98JD00692, 1998.

Flannigan, M. D., Krawchuk, M. A., de Groot, W. J., Wotton, B. M., and Gowman, L. M.: Implications of changing climate for global wildland fire, International Journal of Wildland Fire, 18, 483-507, http://dx.doi.org/10.1071/WF08187, 2009.

Fountoukis, C., and Nenes, A.: ISORROPIA II: a computationally efficient thermodynamic equilibrium model for K+-Ca2+-Mg2+-Nh(4)(+)-Na+-SO42--NO3--Cl--H2O aerosols, Atmos Chem Phys, 7, 4639-4659, 2007.

Freitas, S. R., Longo, K. M., Chatfield, R., Latham, D., Silva Dias, M. A. F., Andreae, M. O., Prins, E., Santos, J. C., Gielow, R., and Carvalho Jr, J. A.: Including the sub-grid scale plume rise of vegetation fires in low resolution atmospheric transport models, Atmos. Chem. Phys., 7, 3385-3398, 10.5194/acp-7-3385-2007, 2007.

Galbally, I. E., Cope, M., Lawson, S. J., Bentley, S. T., Cheng, M., Gillet, R. W., Selleck, P., Petraitis, B., Dunne, E., and Lee, S.: Sources of Ozone Precursors and Atmospheric Chemistry in a Typical Australian City, 2008. http://olr.npi.gov.au/atmosphere/airquality/publications/pubs/ozone-precursors.pdf

Galbally, I. E., Meyer, C. P., Bentley, S. T., Lawson, S. J., and Baly, S. B.: Reactive gases in near surface air at Cape Grim, 2005-2006 – I E Galbally, C P Meyer, S T Bentley, Baseline Atmospheric Program Australia 2005-2006, 77-79, 2007.

Giglio, L., Randerson, J. T., and van der Werf, G. R.: Analysis of daily, monthly, and annual burned area using the fourth-generation global fire emissions database (GFED4), Journal of Geophysical Research: Biogeosciences, 118, 317-328, 10.1002/jgrg.20042, 2013.

Gong, S. L.: A parameterization of sea-salt aerosol source function for sub- and super-micron particles, Global Biogeochem Cy, 17, Artn 1097 Doi 10.1029/2003gb002079, 2003.

Gras, J. L.: Particles Program Report, Baseline Atmospheric Program Australia 2005-2006, 85-86, 2007.

Goodrick, S. L., Achtemeier, G. L., Larkin, N. K., Liu, Y., and Strand, T. M.: Modelling smoke transport from wildland fires: a review, International Journal of Wildland Fire, 22, 83, 10.1071/wf11116, 2013.

Hecobian, A., Liu, Z., Hennigan, C. J., Huey, L. G., Jimenez, J. L., Cubison, M. J., Vay, S., Diskin, G. S., Sachse, G. W., Wisthaler, A., Mikoviny, T., Weinheimer, A. J., Liao, J., Knapp, D. J., Wennberg, P. O., Kurten, A., Crounse, J. D., St Clair, J., Wang, Y., and Weber, R. J.: Comparison of chemical characteristics of 495 biomass burning plumes intercepted by the NASA DC-8 aircraft during the ARCTAS/CARB-2008 field campaign, Atmospheric Chemistry and Physics, 11, 13325-13337, 10.5194/acp-11-13325-2011, 2012.

Hess, G. D.: A photochemical model for air quality assessment: Model description and verification, Atmospheric Environment (1967), 23, 643-660, http://dx.doi.org/10.1016/0004-6981(89)90013-9, 1989.

Hurley, P.: Development and Verification of TAPM, in: Air Pollution Modeling and Its Application XIX, edited by: Borrego, C., and Miranda, A. I., Springer Netherlands, Dordrecht, 208-216, 2008a.

Hurley, P. J.: TAPM V4. Part 1. Technical description, CSIRO Marine and Atmospheric Research Internal Report, 2008b.

Jaffe, D. A., and Wigder, N. L.: Ozone production from wildfires: A critical review, Atmospheric Environment, 51, 1-10, 10.1016/j.atmosenv.2011.11.063, 2012.

Jost, C., Trentmann, J., Sprung, D., Andreae, M. O., McQuaid, J. B., and Barjat, H.: Trace gas chemistry in a young biomass burning plume over Namibia: Observations and model simulations, Journal of Geophysical Research-Atmospheres, 108, 13, 8482 10.1029/2002jd002431, 2003.

Kaiser, J. W., Heil, A., Andreae, M. O., Benedetti, A., Chubarova, N., Jones, L., Morcrette, J. J., Razinger, M., Schultz, M. G., Suttie, M., and van der Werf, G. R.:

Biomass burning emissions estimated with a global fire assimilation system based on observed fire radiative power, Biogeosciences, 9, 527-554, 10.5194/bg-9-527-2012, 2012.

Keywood, M., Guyes, H., Selleck, P., and Gillett, R.: Quantification of secondary organic aerosol in an Australian urban location, Environmental Chemistry, 8, 115-126, 10.1071/en10100, 2011a.

Keywood, M., Kanakidou, M., Stohl, A., Dentener, F., Grassi, G., Meyer, C. P., Torseth, K., Edwards, D., Thompson, A., Lohmann, U., and Burrows, J. P.: Fire in the Air-Biomass burning impacts in a changing climate, Critical Reviews in Environmental Science and Technology, DOI:10.1080/10643389.2011.6042482011b.

Keywood, M., Cope, M., Meyer, C. P. M., Iinuma, Y., and Emmerson, K.: When smoke comes to town: The impact of biomass burning smoke on air quality, Atmospheric Environment, 121, 13-21, http://dx.doi.org/10.1016/j.atmosenv.2015.03.050, 2015.

Korontzi, S., Ward, D. E., Susott, R. A., Yokelson, R. J., Justice, C. O., Hobbs, P. V., Smithwick, E. A. H., and Hao, W. M.: Seasonal variation and ecosystem dependence of emission factors for selected trace gases and PM2.5 for southern African savanna fires, Journal of Geophysical Research: Atmospheres, 108, n/a-n/a, 10.1029/2003JD003730, 2003.

Krummel, P. B., Fraser, P., Steele, L. P., Porter, L. W., Derek, N., Rickard, C., Dunse, B. L., Langenfelds, R. L., Miller, B. R., Baly, S. B., and McEwan, S.: The AGAGE in situ program for non-CO2 greenhouse gases at Cape Grim, 2005-2006: methane, nitrous oxide, carbon monoxide, hydrogen, CFCs, HCFCs, HFCs, PFCs, halons, chlorocarbons, hydrocarbons and sulphur hexafluoride, Baseline Atmospheric Program Australia 2005-2006, 2007.

Lawson, S. J., Keywood, M. D., Galbally, I. E., Gras, J. L., Cainey, J. M., Cope, M. E., Krummel, P. B., Fraser, P. J., Steele, L. P., Bentley, S. T., Meyer, C. P., Ristovski, Z., and Goldstein, A. H.: Biomass burning emissions of trace gases and particles in marine air at Cape Grim, Tasmania, Atmos. Chem. Phys., 15, 13393-13411, 10.5194/acp-15-13393-2015, 2015.

Lei, W., Li, G., and Molina, L. T.: Modeling the impacts of biomass burning on air quality in and around Mexico City, Atmospheric Chemistry and Physics, 13, 2299-2319, 10.5194/acp-13-2299-2013, 2013.

Lu, H., and Shao, Y. P.: A new model for dust emission by saltation bombardment, J Geophys Res-Atmos, 104, 16827-16841, Doi 10.1029/1999jd900169, 1999.

Luhar, A. K., Mitchell, R. M., Meyer, C. P., Qin, Y., Campbell, S., Gras, J. L., and Parry, D.: Biomass burning emissions over northern Australia constrained by aerosol measurements: II—Model validation, and impacts on air quality and radiative forcing, Atmospheric Environment, 42, 1647-1664, http://dx.doi.org/10.1016/j.atmosenv.2007.12.040, 2008.

Mason, S. A., Trentmann, J., Winterrath, T., Yokelson, R. J., Christian, T. J., Carlson, L. J., Warner, T. R., Wolfe, L. C., and Andreae, M. O.: Intercomparison of Two Box Models of the Chemical Evolution in Biomass-Burning Smoke Plumes, Journal of Atmospheric Chemistry, 55, 273-297, 10.1007/s10874-006-9039-5, 2006.

McGregor, J. L.: Recent developments in variable-resolution global climate modelling, Climatic Change, 129, 369-380, 10.1007/s10584-013-0866-5, 2015.

Meyer, C. P., Luhar, A. K., and Mitchell, R. M.: Biomass burning emissions over northern Australia constrained by aerosol measurements: I—Modelling the distribution of hourly emissions, Atmospheric Environment, 42, 1629-1646, http://dx.doi.org/10.1016/j.atmosenv.2007.10.089, 2008.

Ortega, A. M., Day, D. A., Cubison, M. J., Brune, W. H., Bon, D., de Gouw, J. A., and Jimenez, J. L.: Secondary organic aerosol formation and primary organic aerosol oxidation from biomass-burning smoke in a flow reactor during FLAME-3, Atmospheric Chemistry and Physics, 13, 11551-11571, 10.5194/acp-13-11551-2013, 2013.

Pacifico, F., Folberth, G. A., Sitch, S., Haywood, J. M., Rizzo, L. V., Malavelle, F. F., and Artaxo, P.: Biomass burning related ozone damage on vegetation over the Amazon forest: a model sensitivity study, Atmos. Chem. Phys., 15, 2791-2804, 10.5194/acp-15-2791-2015, 2015.

Parrington, M., Palmer, P. I., Henze, D. K., Tarasick, D. W., Hyer, E. J., Owen, R. C., Helmig, D., Clerbaux, C., Bowman, K. W., Deeter, M. N., Barratt, E. M., Coheur, P. F., Hurtmans, D., Jiang, Z., George, M., and Worden, J. R.: The influence of boreal biomass burning emissions on the distribution of tropospheric ozone over North America and the North Atlantic during 2010, Atmospheric Chemistry and Physics, 12, 2077-2098, 10.5194/acp-12-2077-2012, 2012.

Paugam, R., Wooster, M., Freitas, S., and Val Martin, M.: A review of approaches to estimate wildfire plume injection height within large-scale atmospheric chemical transport models, Atmos. Chem. Phys., 16, 907-925, 10.5194/acp-16-907-2016, 2016.

Reid, C. E., Brauer, M., Johnston, F. H., Jerrett, M., Balmes, J. R., and Elliott, C. T.: Critical Review of Health Impacts of Wildfire Smoke Exposure, Environmental health perspectives, 124, 1334-1343, 10.1289/ehp.1409277, 2016.

Reid, J. S., Hyer, E. J., Prins, E. M., Westphal, D. L., Zhang, J., Wang, J., Christopher, S. A., Curtis, C. A., Schmidt, C. C., Eleuterio, D. P., Richardson, K. A., and Hoffman, J. P.: Global Monitoring and Forecasting of Biomass-Burning Smoke: Description of and Lessons From the Fire Locating and Modeling of Burning Emissions (FLAMBE) Program, IEEE Journal of Selected Topics in Applied Earth Observations and Remote Sensing, 2, 144-162, 10.1109/JSTARS.2009.2027443, 2009.

Reisen, F., Meyer, C. P., McCaw, L., Powell, J. C., Tolhurst, K., Keywood, M. D., and Gras, J. L.: Impact of smoke from biomass burning on air quality in rural communities in southern Australia, Atmospheric Environment, 45, 3944-3953, 10.1016/j.atmosenv.2011.04.060, 2011.

Reisen, F., Duran, S. M., Flannigan, M., Elliott, C., and Rideout, K.: Wildfire smoke and public health risk, International Journal of Wildland Fire, 24, 1029, 10.1071/wf15034, 2015.

Sarwar, G., Luecken, D., Yarwood, G., Whitten, G. Z., and Carter, W. P. L.: Impact of an updated carbon bond mechanism on predictions from the CMAQ modeling system: Preliminary assessment, J Appl Meteorol Clim, 47, 3-14, Doi 10.1175/2007jamc1393.1, 2008.

Sarwar, G., Appel, K. W., Carlton, A. G., Mathur, R., Schere, K., Zhang, R., and Majeed, M. A.: Impact of a new condensed toluene mechanism on air quality model predictions in the US, Geosci Model Dev, 4, 183-193, DOI 10.5194/gmd-4-183-2011, 2011.

Seinfeld, J. H., and Pandis, S. N.: Atmospheric chemistry and physics : from air pollution to climate change, Wiley, New York, xxvii, 1326 p. pp., 1998.

Smagorinsky, J.: General circulation experiments with the primitive equations Monthly Weather Review, 91, 99-164, doi:10.1175/1520-0493(1963)091<0099:GCEWTP>2.3.CO;2, 1963.

Trentmann, J., Yokelson, R. J., Hobbs, P. V., Winterrath, T., Christian, T. J., Andreae, M. O., and Mason, S. A.: An analysis of the chemical processes in the smoke plume from a savanna fire, Journal of Geophysical Research-Atmospheres, 110, 20, D12301 10.1029/2004jd005628, 2005.

Tsimpidi, A. P., Karydis, V. A., Zavala, M., Lei, W., Molina, L., Ulbrich, I. M., Jimenez, J. L., and Pandis, S. N.: Evaluation of the volatility basis-set approach for the simulation of organic aerosol formation in the Mexico City metropolitan area, Atmos Chem Phys, 10, 525-546, 2010.

Urbanski, S. P.: Combustion efficiency and emission factors for wildfire-season fires in mixed conifer forests of the northern Rocky Mountains, US, Atmos. Chem. Phys., 13, 7241-7262, 10.5194/acp-13-7241-2013, 2013.

van Leeuwen, T. T., and van der Werf, G. R.: Spatial and temporal variability in the ratio of trace gases emitted from biomass burning, Atmospheric Chemistry and Physics, 11, 3611-3629, 10.5194/acp-11-3611-2011, 2011.

van Leeuwen, T. T., Peters, W., Krol, M. C., and van der Werf, G. R.: Dynamic biomass burning emission factors and their impact on atmospheric CO mixing ratios, Journal of Geophysical Research-Atmospheres, 118, 6797-6815, 10.1002/jgrd.50478, 2013.

Walcek, C. J.: Minor flux adjustment near mixing ratio extremes for simplified yet highly accurate monotonic calculation of tracer advection, Journal of Geophysical Research: Atmospheres, 105, 9335-9348, 10.1029/1999JD901142, 2000.

Wigder, N. L., Jaffe, D. A., and Saketa, F. A.: Ozone and particulate matter enhancements from regional wildfires observed at Mount Bachelor during 2004-2011, Atmospheric Environment, 75, 24-31, 10.1016/j.atmosenv.2013.04.026, 2013.

Yokelson, R. J., Bertschi, I. T., Christian, T. J., Hobbs, P. V., Ward, D. E., and Hao, W. M.: Trace gas measurements in nascent, aged, and cloud-processed smoke from African savanna fires by airborne Fourier transform infrared spectroscopy (AFTIR), Journal of Geophysical Research-Atmospheres, 108, 8478 10.1029/2002jd002322, 2003.

Yokelson, R. J., Karl, T., Artaxo, P., Blake, D. R., Christian, T. J., Griffith, D. W. T., Guenther, A., and Hao, W. M.: The Tropical Forest and Fire Emissions Experiment: overview and airborne fire emission factor measurements, Atmospheric Chemistry and Physics, 7, 5175-5196, 2007.

Yokelson, R. J., Crounse, J. D., DeCarlo, P. F., Karl, T., Urbanski, S., Atlas, E., Campos, T., Shinozuka, Y., Kapustin, V., Clarke, A. D., Weinheimer, A., Knapp, D. J., Montzka, D. D., Holloway, J., Weibring, P., Flocke, F., Zheng, W., Toohey, D., Wennberg, P. O., Wiedinmyer, C., Mauldin, L., Fried, A., Richter, D., Walega, J., Jimenez, J. L., Adachi, K., Buseck, P. R., Hall, S. R., and Shetter, R.: Emissions from biomass burning in the Yucatan, Atmospheric Chemistry and Physics, 9, 5785-5812, 2009.

Yokelson, R. J., Burling, I. R., Urbanski, S. P., Atlas, E. L., Adachi, K., Buseck, P. R., Wiedinmyer, C., Akagi, S. K., Toohey, D. W., and Wold, C. E.: Trace gas and particle

emissions from open biomass burning in Mexico, Atmospheric Chemistry and Physics, 11, 6787-6808, 10.5194/acp-11-6787-2011, 2011.

970

971 **Table 1. EF used in model sensitivity studies, corresponding to low (MCE=0.89), medium (MCE=0.92) and**
972 **high (MCE = 0.95) MCEs. A subset of the total species included in the CB05 lumped chemical mechanism**
973 **are shown. Also shown are savannah EF from Andreae and Merlet (2001) (A&M) and EF calculated from**
974 **BB2 in previous work (Lawson et al., 2015). NO = nitric oxide, CO =carbon monoxide, PAR=paraffin**
975 **carbon bond, OLE= terminal olefin carbon bond, TOL=toluene and other monoalkyl aromatics,**
976 **XYL=xylene and other polyalkyl aromatics, BNZ =benzene, FORM=formaldehyde, ALD2=acetaldehyde,**
977 **EC=elemental carbon <10 µm, OC=primary organic carbon < 10 µm**

978

979

980

	EF g kg $^{-1}$				
	A&M (2001)	Lawson et al., (2015)	Used in this work		
	MCE 0.94	MCE 0.88	MCE 0.89	MCE 0.92	MCE 0.95
NO	3.9	n/a	0.8	2.7	4.7
CO	65	127	121	89	57
PAR	1.55	n/a	2.33	2.02	1.40
OLE	0.54	n/a	0.81	0.7	0.49
TOL	0.2	0.30	0.3	0.26	0.18
XYL	0.045	0.26	0.07	0.06	0.04
BNZ	0.23	0.69	0.35	0.3	0.21
FORM	0.42	1.64	0.63	0.55	0.38
ALD2	0.5	0.92	0.75	0.65	0.45
EC	0.48	0.16	0.19	0.34	0.53
OC	3.40	n/a	5.10	4.08	3.06
NMOC/NO_x	1.60	n/a	11.99	2.97	1.20

981

Table 2. Summary of sensitivity study results, including Meteorology, Emission Factors and Spatial Variability.

Sensitivity study	Species	TAPM-CTM simulation	CCAM-CTM simulation	Comments/drivers of model outputs
Meteorology (Section 3.1.1)	BC and CO	BB1 plume strike +3 hr Duration 12 hr (actual 5 hr)	BB1 plume strike -12 hr Duration 36 hr intermittent (actual 5 hr)	Narrow BB plume. Differences in plume strike due to timing of wind direction change; windspeeds; direct or indirect advection of plume over Cape Grim
		BB2 plume strike -26 hr Duration 50 hr (actual 29 hr)	BB2 plume strike -26 hr Duration 57 hr (actual 29 hr)	Wind direction differences driven by gravity wave oscillations;timing of wind direction change; different wind speeds driving absolute BB emissions and plume dispersion
	O_3	4 O_3 peaks simulated (2 observed, 2 not)	1 O_3 peak simulated (observed)	Differences in simulated wind speed and direction (and EF – see below)
Emission Factors (Section 3.1.2)	BC and CO	BC peak magnitude varies by factor 3, CO factor 2 with different EF runs	As for TAPM -CTM	Concentrations vary according to EF input ratios.
	O_3	2 peaks with high EF sensitivity, 2 peaks with no EF sensitivity	1 peak with no EF sensitivity	Different NMOC/NO_x emission ratios (varies with MCE) drives destruction or production of O_3 in fire related peaks. MCE 0.89 TAPM-CTM simulation gives best agreement with observations
Spatial Variability (Section 3.1.3)	CO	Differences of up to > 500 ppb in grid points 1 km apart (BB2)	n/a	Narrow BB plume
	O_3	Differences of up to 15 ppb in grid points 1 km apart (BB1)	n/a	Narrow ozone plume generated downwind of fire

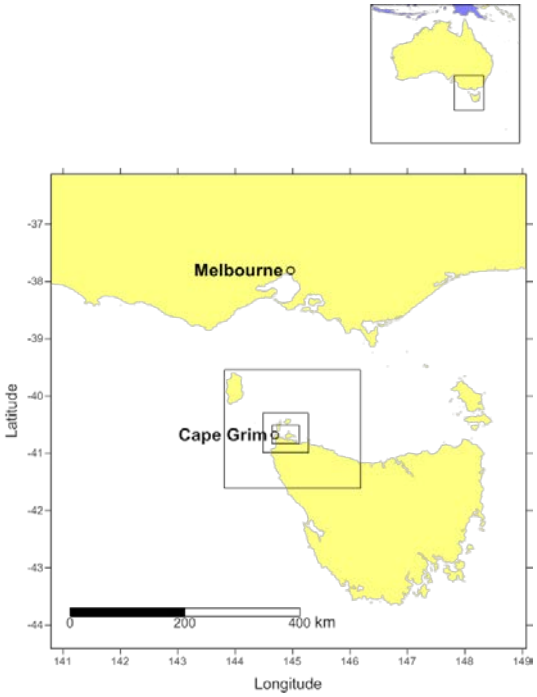

Figure 1. The five nested computational domains used in TAPM-CTM and CCAM-CTM, showing cell spacings of 20 km, 12 km, 3 km, 1 km and 400 m.

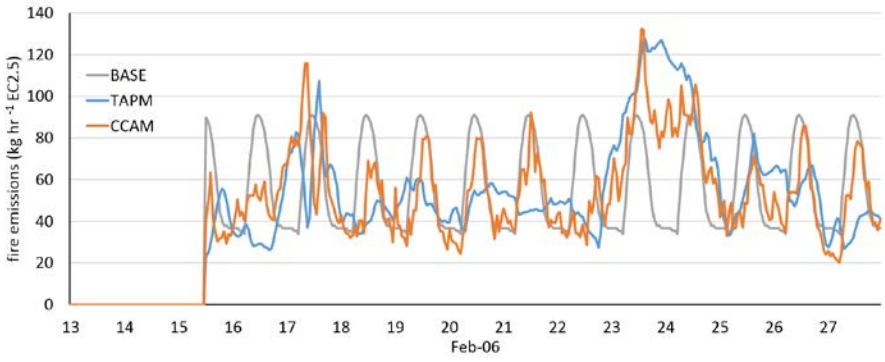

Figure 2 Base hourly diurnal emissions and revised Macarthur Fire Danger Index (FDI)-scale emissions generated using TAPM and CCAM meteorology.

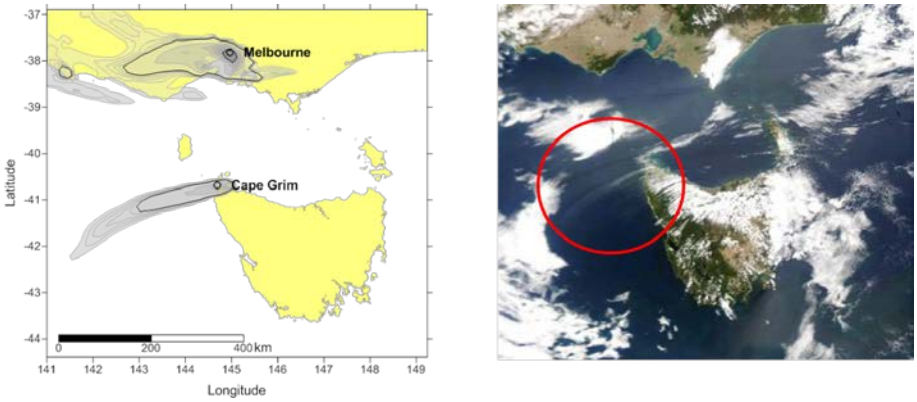

Figure 3. Model output of BC (left) on the 23rd February, with a MODIS Truecolour image of the same period.

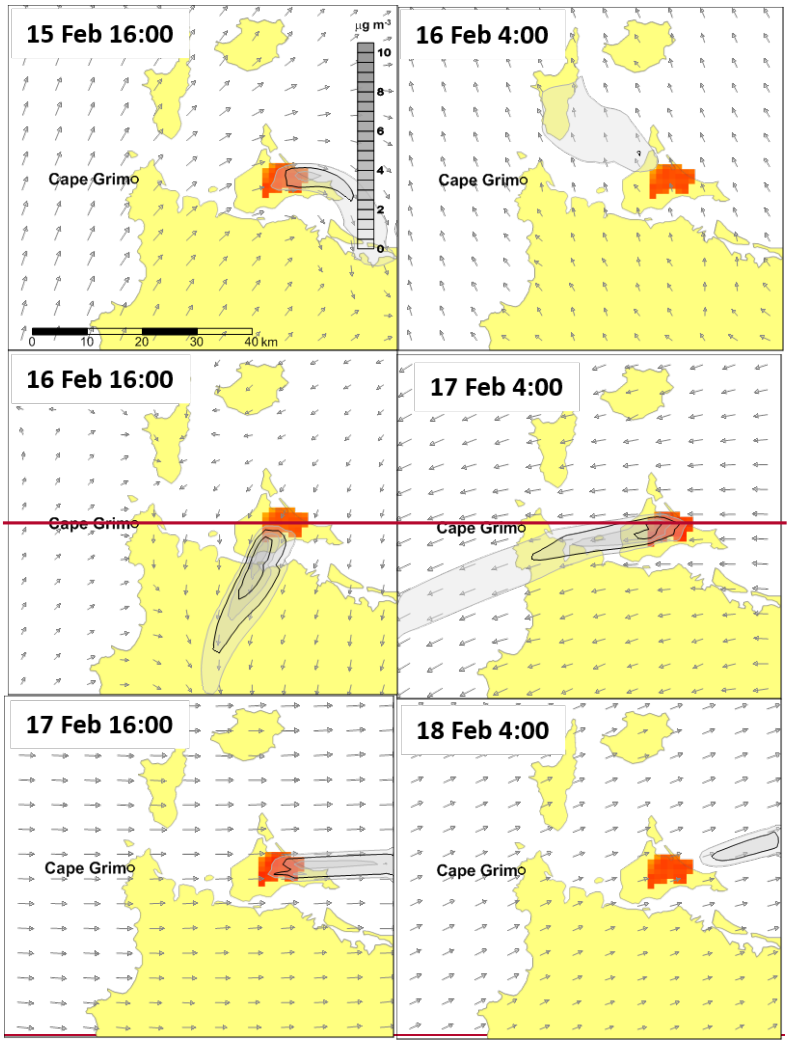
15 Feb 16:00
µg m-3
10
8
6
4
2
0
Cape Grimo
0 10 20 30 40 km
16 Feb 4:00
Cape Grimo
16 Feb 16:00
Cape Grimo
17 Feb 4:00
Cape Grimo
17 Feb 16:00
Cape Grimo
18 Feb 4:00
Cape Grimo

17

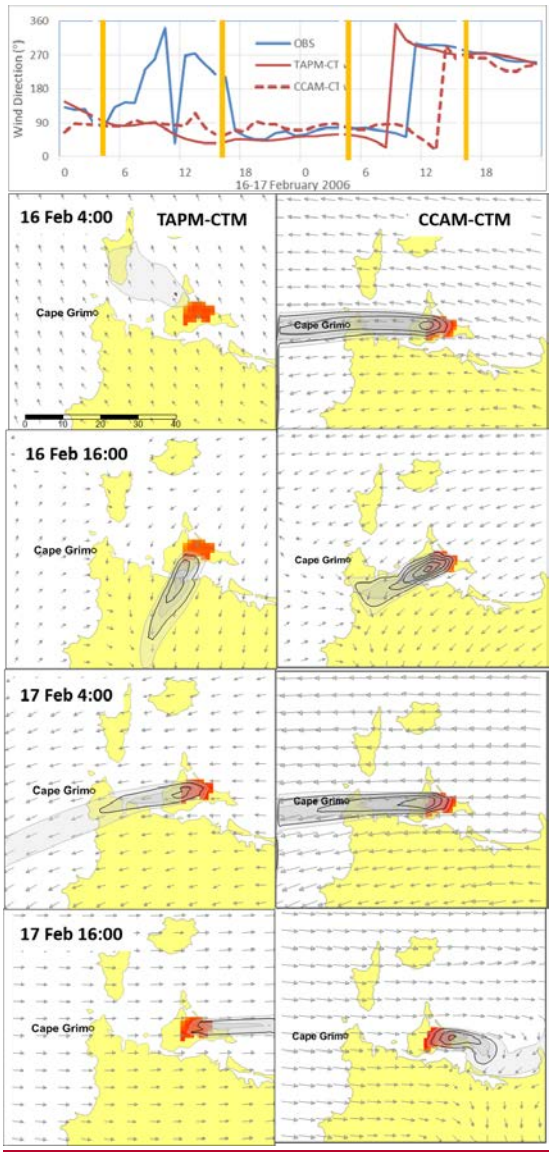

Figure 4. Model concentration isopleth of BC for TAPM-CTM (left panels) and CCAM-CTM (right panels). Panels show ~~Model output of BC~~ for ~~TAPM-CTM at~~ 12 hour time intervals during BB1, ~~showing~~ including the Robbins Island BB plume intermittently striking Cape Grim, and then the change in plume direction with wind direction change. Arrows are wind vectors. The time series of observed and modelled wind direction for BB1 is shown above with orange bands highlighting the periods corresponding to the panels.

Formatted: Not Highlight

Formatted: Not Highlight

Formatted: Not Highlight

~~Model output of BC for CCAM-CTM at 12 hour time intervals during BB1, showing the Robbins Island BB plume intermittently striking Cape Grim, and then the change in plume direction with wind direction change. Arrows are wind vectors.~~

Formatted: Normal

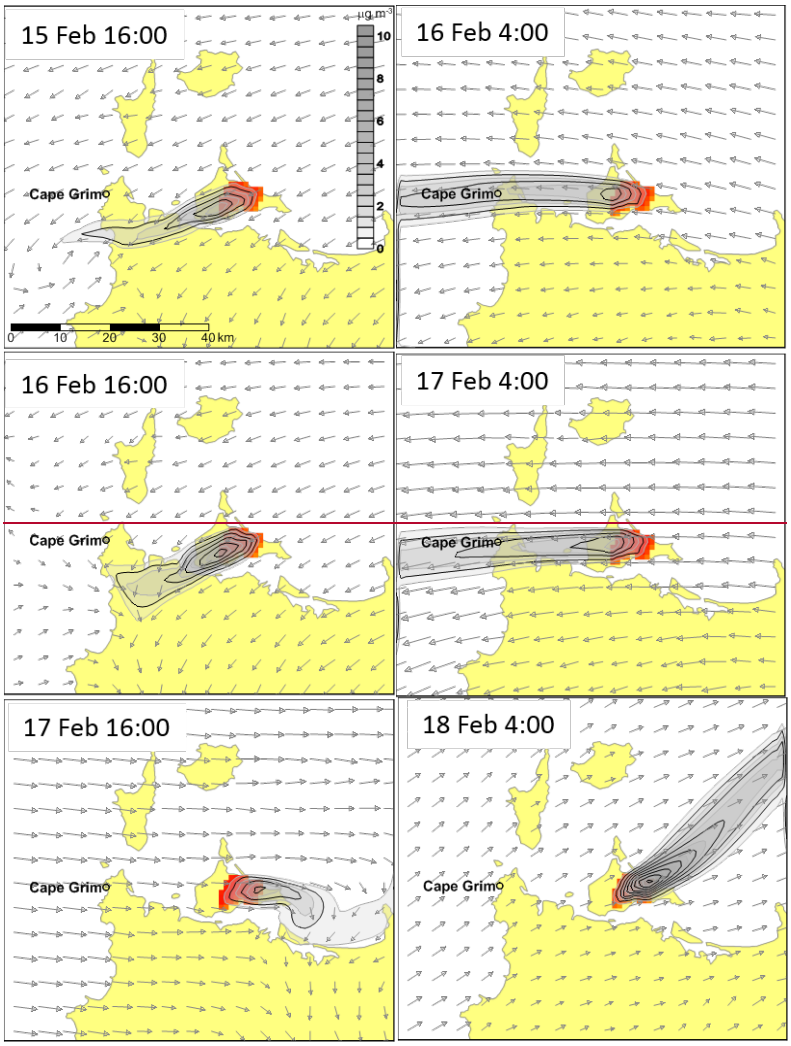
15 Feb 16:00
µg.m-3
10
8
6
4
2
0
Cape Grimo
0 10 20 30 40 km
16 Feb 4:00
Cape Grimo
16 Feb 16:00
Cape Grimo
17 Feb 4:00
Cape Grimo
17 Feb 16:00
Cape Grimo
18 Feb 4:00
Cape Grimo

29

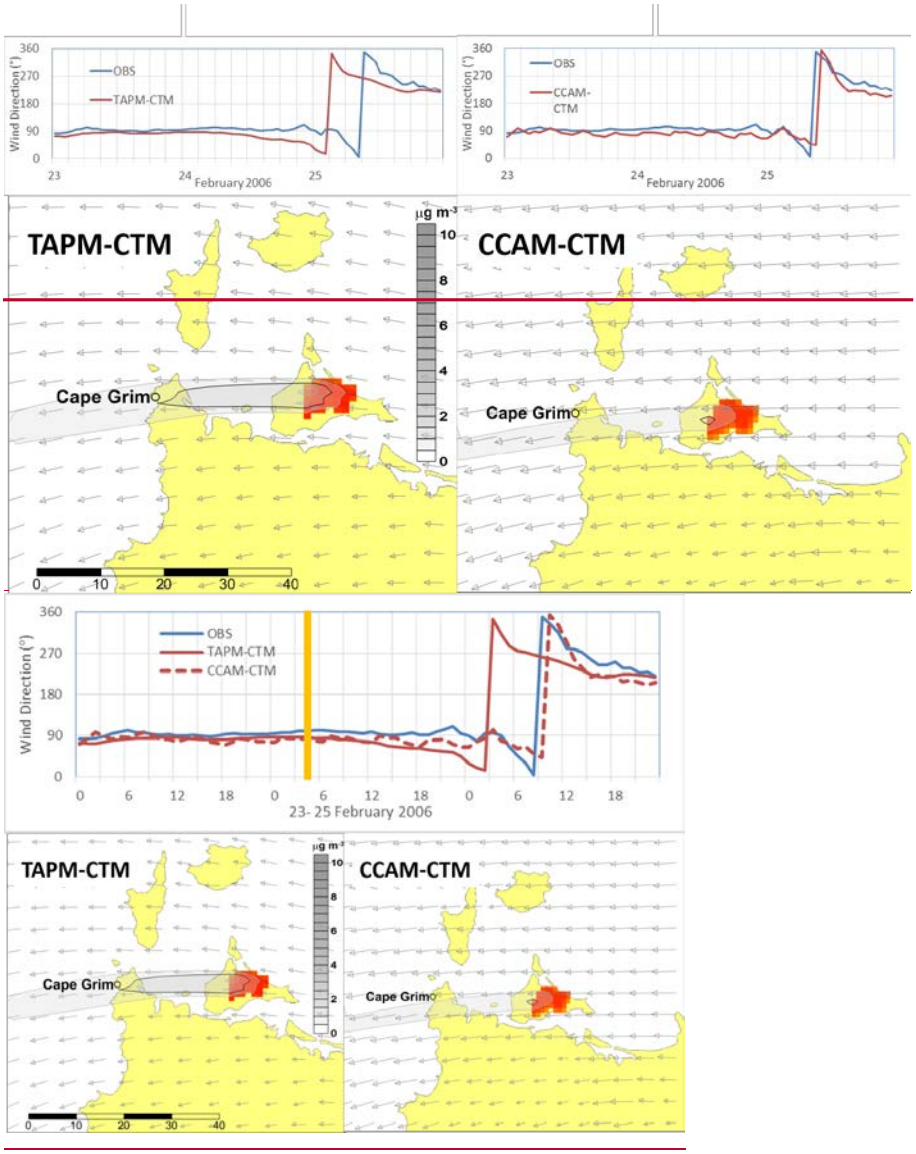

Figure 5 Model ~~C~~concentration isopleth of BC ~~and Wind direction~~ for TAPM-CTM and CCAM-CTM at 05:00 on the 24 February during BB2. Arrows are wind vectors. The time series of observed and modelled wind direction for BB2 is shown above with an orange band highlighting the period corresponding to the panels.

Formatted: Not Highlight

Formatted: Not Highlight

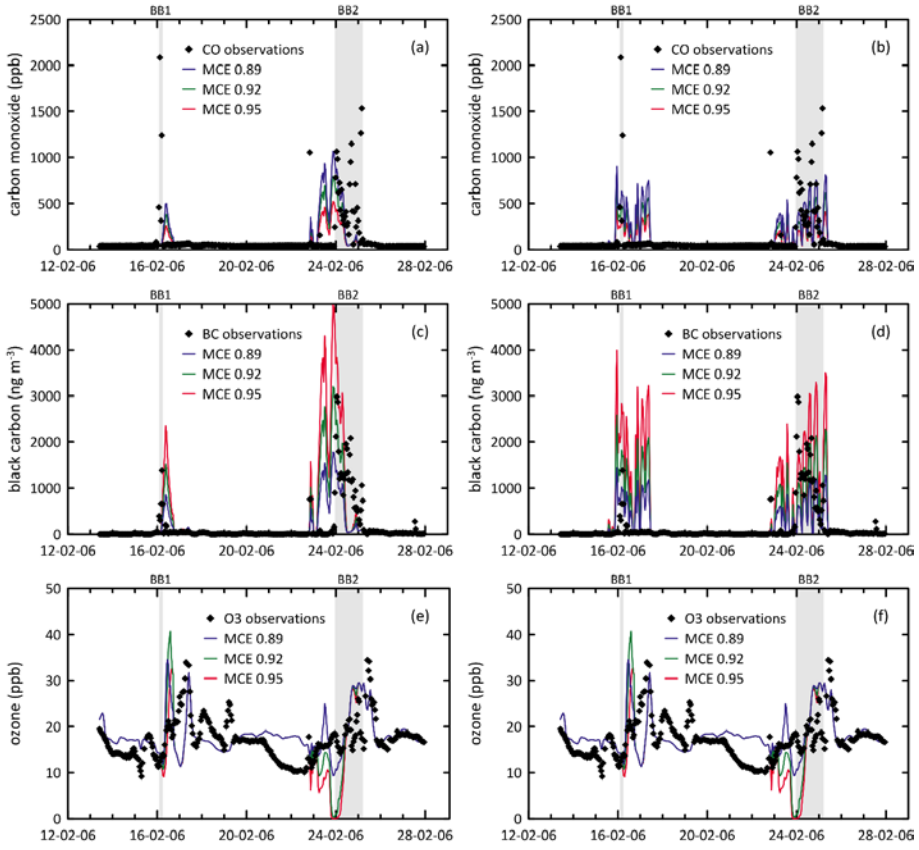

Figure 6. Simulated CO using a) TAPM-CTM and b) CCAM-CTM, simulated BC using c) TAPM-CTM and d) CCAM-CTM, and simulated O_3 using e) TAPM-CTM and f) CCAM-CTM. Coloured lines represent different MCE EF simulations, black symbols are observations

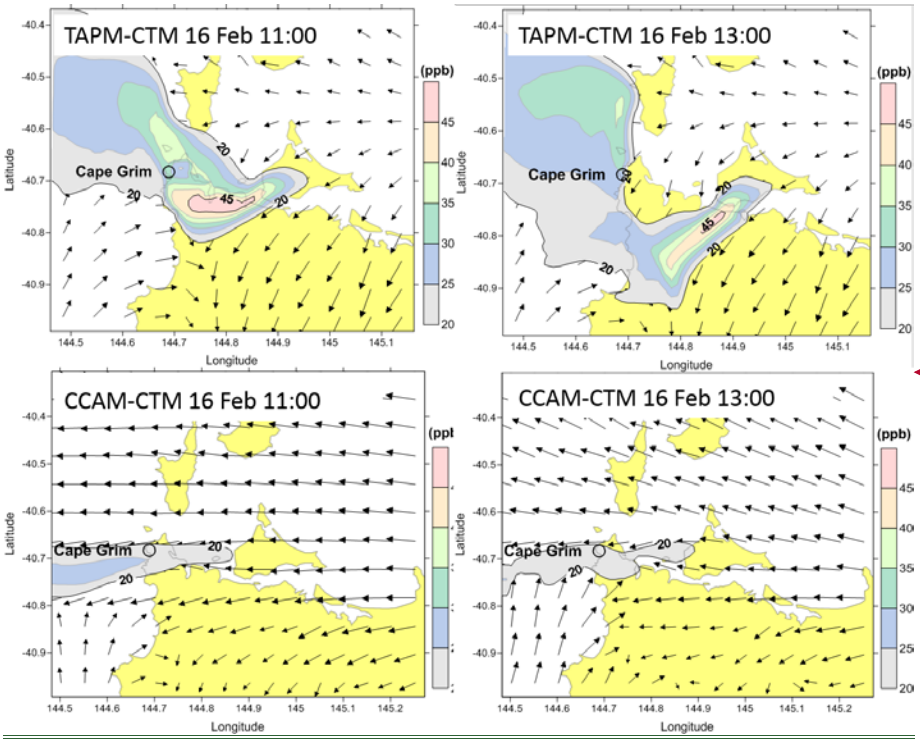

Figure 7 Model output showing O_3 enhancement downwind of the fire during BB1 at 11:00 and 13:00 on the 16 February for TAPM-CTM (top) and CCAM-CTM (bottom). The spatially variable plume and complex wind fields are shown. Arrows are wind vectors.

Formatted: Keep with next

Formatted: Caption

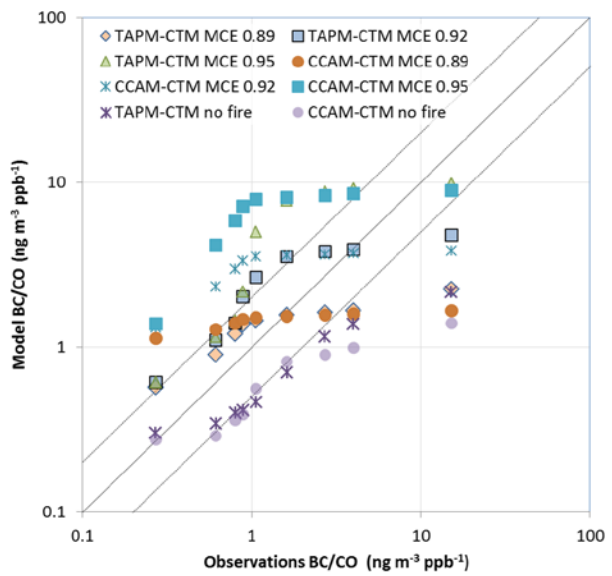

Figure 8 Quantile-quantile plots of observed and modelled BC/CO ratios for the TAPM-CTM and CCAM-CTM simulations. For each scenario, the model-data pairs correspond to the following percentiles- 0.2, 0.3, 0.4, 0.5, 0.6, 0.7, 0.8, 0.9 and 1. Note log scale on both axes. Solid line is 1:1 and dotted lines show performance within a factor of two.

Formatted: Keep with next

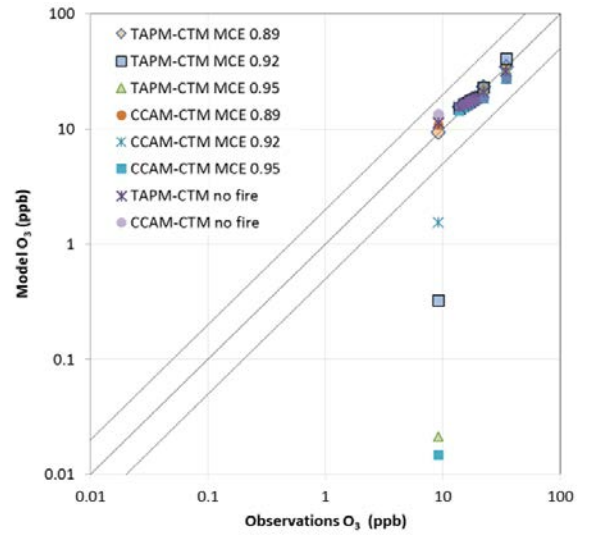

Figure 9 Quantile-quantile plots of observed and modelled O_3 for the TAPM-CTM and CCAM-CTM simulations. For each scenario, the model-data pairs correspond to the following percentiles- 0.2, 0.3, 0.4, 0.5, 0.6, 0.7, 0.8, 0.9 and 1. Note log scale on both axes. Solid line is 1:1 and dotted lines show performance within a factor of two.

Formatted: Keep with next

Formatted: Caption

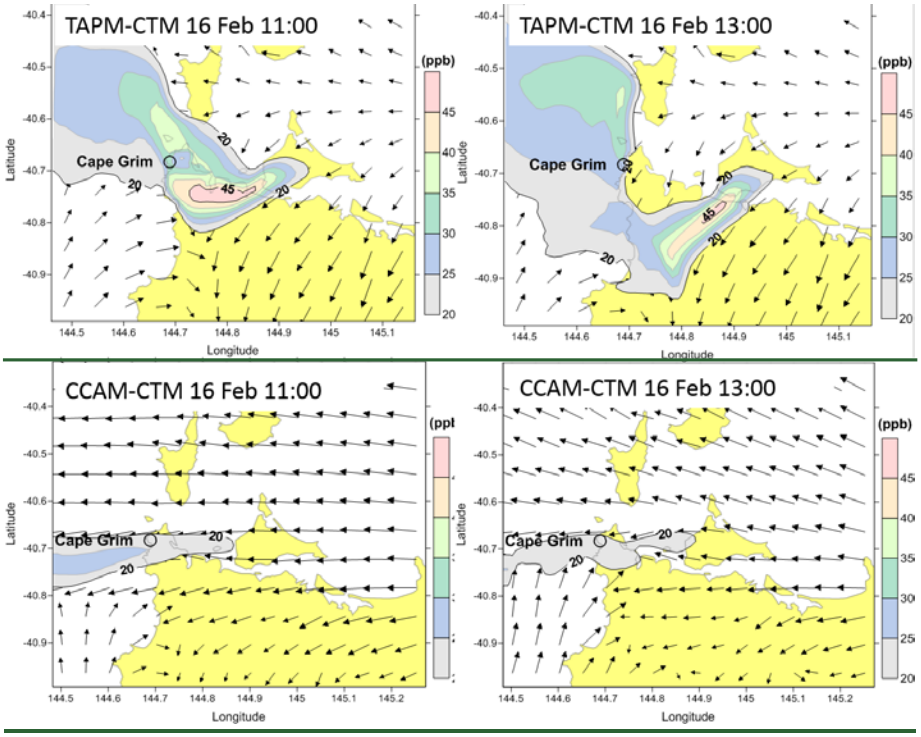
TAPM-CTM 16 Feb 11:00
TAPM-CTM 16 Feb 13:00
CCAM-CTM 16 Feb 11:00
CCAM-CTM 16 Feb 13:00
Cape Grim
Latitude
Longitude
(ppb)

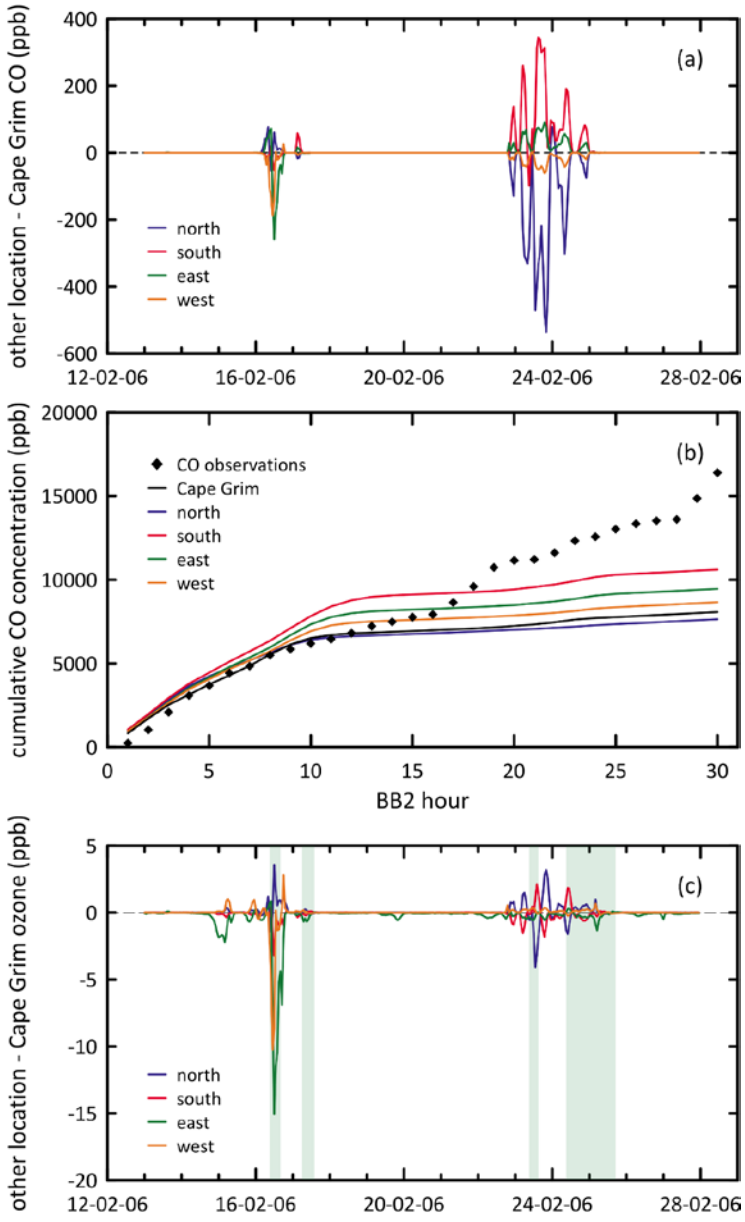

Figure 10 Simulated spatial variability using TAPM-CTM with MCE=0.89 showing a) time series of CO over two weeks of fire (BB1 and BB2 shown), b) the observed and modelled cumulative concentration of CO over the 29 hour duration of BB2 and c) time series of O_3 over the two weeks of fire. The four modelled O_3 peaks in the Cape Grim gridpoint are shaded. Figs a and c show the difference between simulated

concentrations at Cape Grim and at 4 surrounding grid points 1km north, south, east and west of Cape Grim.Fig b shows simulated cumulative CO at Cape Grim and at 4 surrounding grid points. . Observations are black symbols.

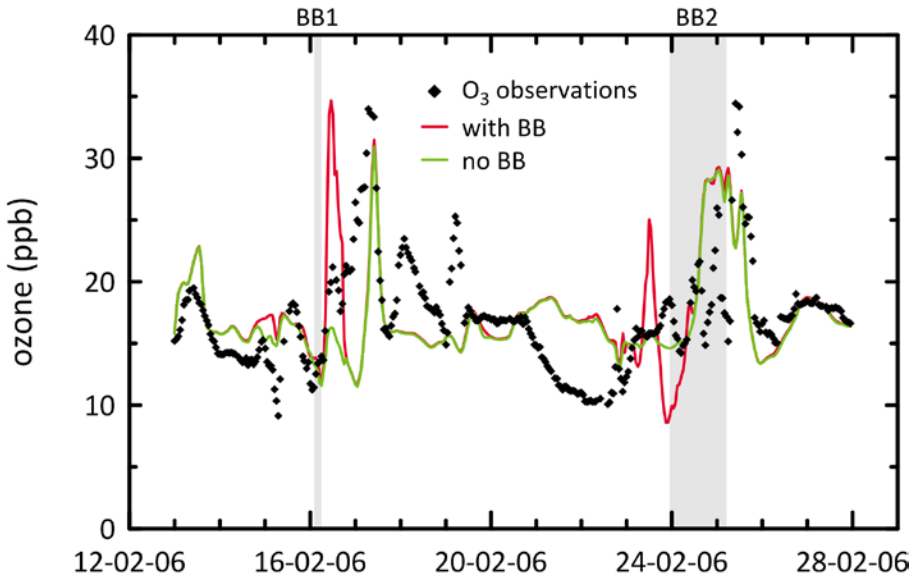

Figure 11 Simulated O_3 concentration at Cape Grim with the Robbins Island fire emissions (red line) and without the fire emissions (green line). Observations are black symbols. Model used was TAPM-CTM with EF corresponding to MCE=0.89. The periods corresponding to observed BB1 and BB2 are shaded.

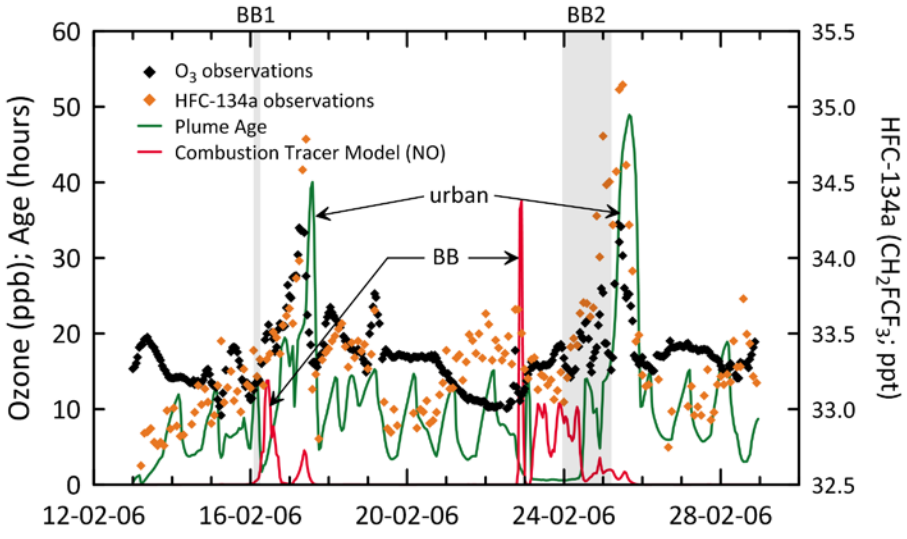

Figure 12 Simulated plume age (green line), simulated combustion tracer (NO) (red line), observed O_3 (black symbols) and observed HFC-134a (orange symbols) over 2 week duration of the fire. The modelled BB periods (red peaks) and impact of urban air from mainland Australia (green peaks) are labelled. The periods corresponding to observed BB1 and BB2 are shaded.

End